Ultrasound
in medicine
and biology

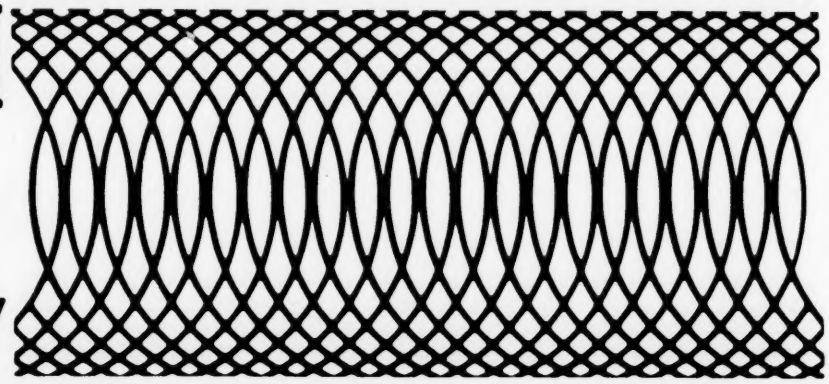

Author–Subject Index
Volume 25 (1999)

Compiled by

Michael Halliwell

Department of Medical Physics, Bristol General Hospital, Bristol BS1 6SY, United Kingdom

ELSEVIER

Ultrasound in Med. & Biol., Vol. 26, pp. 679–728, 2000
Copyright © 2000 World Federation for Ultrasound in Medicine & Biology
Printed in the USA. All rights reserved
0301-5629/00/$–see front matter

ELSEVIER

AUTHOR/SUBJECT INDEX

3D

3D
2-D and 3-D endoluminal ultrasound: vascular and nonvascular applications (Liu), 159
3-D power Doppler cerebral angiography in neonates and young infants: comparison with 2-D power Doppler angiography (Peng), 947
3-D ultrasound quantification of neonatal cerebral ventricles in different head positions (Nagdyman), 895
dynamic three-dimensional freehand echocardiography using raw digital ultrasound data (Berg), 745
effect of catheter placement on 3-D velocity profiles in curved tubes resembling the human coronary system (Krams), 803
effect of ECHO contrast media on the visualization of transverse sinus thrombosis with transcranial 3-D duplex sonography (Delcker), 1063
forty years of obstetric ultrasound 1957-1997: from A-scope to three dimensions (McNay), 3 (Historical Review)
morphological evaluation of a regurgitant orifice by 3-D echocardiography: applications in the quantification of valvular regurgitation (Anayiotos), 209
noninvasive 3-D ultrasound of atherosclerotic plaques in the Watanabe rabbit (Allott), 905
semiautomatic registration of volumetric ultrasound scans (Meyer), 339
SieScape™ images (Nock), 861 (Letter)
the axolotl as an animal model for the comparison of 3-D ultrasound with plain film radiography (Kulbisky), 969
the fetal spinal canal - a three-dimensional study (Wallny), 1329

A

Abbott, J. G.: rationale and derivation of MI and TI – a review, 431
Abraham, P., Ternisien, C., Hubert, L., Pidhorz, L. and Saumet, J.-L.: does venous microemboli detection add to the interpretation of D-dimer values following orthopedic surgery?, 637 (Clinical Note)
Abraham, P., see Roy, E.

accuracy
a rotating torus phantom for assessing color Doppler accuracy (Stewart), 1251
a validation study on the intraobserver and interobserver reproducibility of renal artery duplex ultrasound (Baumgartner), 225
accuracy of the main Doppler methods for evaluating the degree of carotid stenoses (continuous wave, pulsed wave, and color Doppler), (Arbeille), 65
application of a semiautomatic boundary detection algorithm for the assessment of amniotic fluid quantity from ultrasound images (Sagiv), 515

color Doppler velocity accuracy proximal to regurgitant orifices: influence of orifice aspect ratio (Myers), 771
comparison of transcranial Doppler flow velocity and cerebral blood flow during focal ischemia in rabbits (Els), 933
increased accuracy of echocardiographic measurement of flow using automated spherical integration of multiple plane velocity vectors (Brandberg), 249
measurement accuracy of the flow velocity in pulsed ultrasound Doppler velocimeter (Kagiyama), 1265
quantitative Doppler measures in coiled vessels: investigation on excised umbilical veins (Guiot), 1465
robustness of integrated backscatter for myocardial tissue characterization (Bijnens), 95
semiautomatic registration of volumetric ultrasound scans (Meyer), 339
variability in ultrasonic measurements of arterial stiffness in the atherosclerosis risk in communities study (Arnett), 175
voltage sensitivity response of ultrasonic hydrophones in the frequency range 0.25-2.5 MHz (Lewin), 1131

Achilles tendons
strain measurements of rabbit Achilles tendons by ultrasound (Kuo), 1241

Ackerstaff, R. G. A., see Mess, W. H.
Ackerstaff, R. G. A., see Montauban van Swijndregt, A. D.

acoustic emission
stimulated acoustic emission to image a late liver and spleen-specific phase of Levovist® in normal volunteers and patients with and without liver disease (Blomley), 1341

acoustic microscopy
relationship between myocardial tissue density measured by microgravimetry and sound speed measured by acoustic microscopy (Masugata), 1459 (Clinical Note)

acoustic non-linearity parameter
acoustic saturation and output regulation (Duck), 1009
experimental investigation of the acoustic nonlinearity parameter tomography for excised pathological biological tissues (Zhang), 593
nonlinear and linear propagation of diagnostic ultrasound pulses (Filipczynski), 285
nonlinearity parameter for tissue-mimicking materials (Dong), 831

acoustic output
intercomparison of acoustic output measurements of a diagnostic ultrasound device (Beissner), 529
voltage sensitivity response of ultrasonic hydrophones in the frequency range 0.25-2.5 MHz (Lewin), 1131

acoustic saturation
acoustic saturation and output regulation (Duck), 1009

acoustic streaming
the use of acoustic streaming in breast lesion diagnosis: a clinical study (Nightingale), 75

Adir, Y., see Shupak, A.

agglutination
ultrasonic enhancement of coated particle agglutination immunoassays: influence of particle density (Thomas), 443

Ahuja, A., see Chan, S.-T.
Ahuja, A., see Ying, M.
Akselrod, S., see Sagiv, C.
Akselrod, S., see Zimmer, Y.
Alam, S. K., see Konofagou, E. E.
Albrecht, K. W., see Schuurman, P. R.
Albrecht, T., see Blomley, M. J. K.
Alcázar, J. L. and Jurado, M.: transvaginal color Doppler for prediting pathologial response to preoperative chemoradiation in locally advanced cervical carcinoma: a preliminary study, 1041
Alderman, J., see Brown, J. M.
Alessandro, J., see Forsberg, F.
Allard, L., Cloutier, G., Guo, Z. and Durand, L.-G.: review of the assessment of single level and multilevel arterial occlusive disease in lower limbs by duplex ultrasound, 495
Allott, C. P., Barry, C. D., Bramley, J., John, N. W., Mellor, P. M., Thomson, D. S. and Reilly, C. F.: noninvasive 3-D ultrasound of atherosclerotic plaques in the Watanabe rabbit, 905

amniotic fluid
application of a semiautomatic boundary detection algorithm for the assessment of amniotic fluid quantity from ultrasound images (Sagiv), 515

Anayiotos, A. S., Smith, B. K., Kolda, M., Fan, P. and Nanda, N. C.: morphological evaluation of a regurgitant orifice by 3-D echocardiography: applications in the quantification of valvular regurgitation, 209
Anayiotos, A. A., see Myers, J. G. Jr.
Anderson, T., see Hoskins, P. R.
Andreoli, S. P., see Williams, J. C. Jr.
Arbeille, P., Bouin-Pineau, M.-H. and Herault, S.: accuracy of the main Doppler methods for evaluating the degree of carotid stenoses (continuous wave, pulsed wave, and color Doppler), 65
Arnett, D. K., Chambless, L. E., Kim, H., Evans, G. W. and Riley, W.: variability in ultrasonic measurements of arterial stiffness in the atherosclerosis risk in communities study, 175
Aydin, N., Padayachee, S. and Markus, H. S.: the use of the wavelet transform to describe embolic signals, 953

artefacts
analysis of flash echo from contrast agent for designing optimal ultrasound diagnostic systems (Kamiyama), 411
application of a semiautomatic boundary detection algorithm for the assessment of amniotic fluid quantity from ultrasound images (Sagiv), 515
modeling geometric artefacts in intravascular ultrasound imaging (Delachartre), 567
signal from hepatic hemangiomas on power Doppler US: real or artefactual? (Kim), 1055

Arieli, R., see Shupak, A.
Arieli, Y., see Shupak, A.
Armentano, R. L., see Graf, S.

artery
artificial neural network analysis of common femoral artery Doppler shift signals: classification of proximal disease (Wright), 735
assessment of coronary stenoses by Doppler wires: a validation study using *in vitro* modeling and computer simulations (Porenta), 793
carotid arterial stiffness as a surrogate for aortic stiffness: relationship between carotid artery pressure-strain elastic modulus and aortic pulse wave velocity (Nagai), 181
clinical implications of online and off-line interobserver variability in intracoronary ultrasound-guided interventions (Smits), 509
decay index: a new carotid Doppler waveform measure associated with the Windkessel function of elastic arteries (Nagai), 1371
evaluation of off-line automated intima-media thickness detection of the common carotid artery - based on M-line signal processing (Willekes), 57
experimental and clinical validation of arterial diameter waveform and intimal media thickness obtained from B-mode ultrasound image processing (Graf), 1353
hemostasis of punctured vessels using Doppler-guided high-intensity ultrasound (Martin), 985
middle cerebral artery anatomy and characteristics of embolic signals: a dual gate computer simulation study (Mess), 531
noninvasive 3-D ultrasound of atherosclerotic plaques in the Watanabe rabbit (Allott), 905
noninvasive assessment of the viscoelasticity of peripheral arteries (Shau), 1377
review of the assessment of single level and multilevel arterial occlusive disease in lower limbs by duplex ultrasound (Allard), 495
the effect of hemodynamics, vessel wall compliance and hematocrit on ultrasonic Doppler power: an *in vitro* study (Missaridis), 549
three months use of third-generation oral contraceptives does not affect artery wall properties (Willekes), 723
variability in ultrasonic measurements of arterial stiffness in the atherosclerosis risk in communities study (Arnett), 175

Ask, P., see Brandberg, J.

attenuation
broadband measurement of the scattering-to-attenuation ratio for Albunex® at 37°C (Marsh), 1321 (Technical Note)
confounding effects of myocardial background intensity and attenuation in contrast echocardiography: an *in vivo* study (Bos), 1177
high-frequency estimation of the ultrasonic attenuation coefficient slope obtained in human skin: simulation and *in vivo* results (Guittet), 421
histological study of normal and tumor-bearing liver treated with focused ultrasound (Chen), 847
on the relation between aggregation, packing and the backscattered ultrasound signal for whole blood (Lim), 1395
on the ultrasonic attenuation and its frequency dependence in the Os Calcis assessed with a multielement receiver (Strelitzki), 133
three months use of third-generation oral contraceptives does not affect artery wall properties (Willekes), 723

ultrasonic propagation in cancellous bone: a new stratified model (Hughes), 811
ultrasound backscatter and attenuation in human liver with diffuse disease (Lu), 1047
wide-band spectroscopy of biological material based on a laser-induced grating technique (Maznev), 601

axolotl
the axolotl as an animal model for the comparison of 3-D ultrasound with plain film radiography (Kulbisky), 969

B

Baccini, F., see Pallotta, N.

backscatter
alterations in ultrasonic backscatter during intra-aortic balloon counterpulsation support in patients with acute myocardial infarction (Liu), 1185
broadband measurement of the scattering-to-attenuation ratio for Albunex® at 37°C (Marsh), 1321 (Technical Note)
dependence of "apparent" magnitude on the time delay of cyclic variation of myocardial backscatter (Finch-Johnston), 759
Doppler backscatter properties of a blood-mimicking fluid for Doppler performance assessment (Ramnarine), 105
echo decorrelation estimated from signal powers (Li), 405
echogenicity of fetal lung and liver quantified by the grey-level histogram width (Maeda), 201
effect of filling gases on the backscatter from contrast microbubbles: theory and *in vivo* measurements (Forsberg), 1203
high-frequency estimation of the ultrasonic attenuation coefficient slope obtained in human skin: simulation and *in vivo* results (Guittet), 421
on the relation between aggregation, packing and the backscattered ultrasound signal for whole blood (Lim), 1395
pressure dependence of subharmonic signals from contrast microbubbles (Shi), 275
robustness of integrated backscatter for myocardial tissue characterization (Bijnens), 95
stimulated acoustic emission to image a late liver and spleen-specific phase of Levovist® in normal volunteers and patients with and without liver disease (Blomley), 1341
the effect of hemodynamics, vessel wall compliance and hematocrit on ultrasonic Doppler power: an *in vitro* study (Missaridis), 549
ultrasonic backscattering from porcine whole blood of varying hematocrit and shear rate under pulsatile flow (Lin), 1151
ultrasonic propagation in cancellous bone: a new stratified model (Hughes), 811
ultrasound backscatter and attenuation in human liver with diffuse disease (Lu), 1047

Bailey, M. R., see Poliachik, S. L.
Bailey, M. R., see Williams, J. C. Jr.
Baker, K. G., see Sirlin, C. B.
Bao, S., see Miller, D. L.
Bao, S., see Miller, D. L.

Barra, J. G., see Graf, S.
Barry, C. D., see Allott, C. P.
Basude, R., see Forsberg, F.
Bauer, A., see Blomley, M. J. K.
Baumgartner, I., Behrendt, P., Rohner, P. and Baumgartner, R. W.: a validation study on the intraobserver and interobserver reproducibility of renal artery duplex ultrasound, 225
Baumgartner, H., see Binder, T.
Baumgartner, H., see Porenta, G.
Baumgartner, R. W., see Baumgartner, I.
Bautista, R., see Lewin, P. A.
Beach, K., see Takayama, K.
Becker, G., see Berg, D.
Becker, G., see Puls, I.
Behrendt, P., see Baumgartner, I.
Behrens, S., Daffertshofer, M., Spiegel, D. and Hennerici, M.: low-frequency, low-intensity ultrasound accelerates thrombolysis through the skull, 269
Beissner, K.: intercomparison of acoustic output measurements of a diagnostic ultrasound device, 529
Beller, K.-D., see Strauss, A. L.
Bensted, J. P. M., see Chen, L.
Berg, D., Grote, C., Rausch, W.-D., Mäurer, M., Wesemann, W., Riederer, P. and Becker, G.: iron accumulation in the substantia nigra in rats visualized by ultrasound, 901
Berg, D., see Müllges, W.
Berg, S., Torp, H., Martens, D., Steen, E., Samstad, S., Høivik, I. and Olstad, B.: dynamic three-dimensional freehand echocardiography using raw digital ultrasound data, 745
Berson, M., see Guittet, C.
Bianco, B., see Luo, G.
Bijnens, B., D'hooge, J. D., Sutherland, G., Herregods, M.-C., Nuyts, J., Suetens, P. and Van de Werf, F.: robustness of integrated backscatter for myocardial tissue characterization, 95
Binder, T., Süssner, M., Moertl, D., Strohmer, T., Baumgartner, H., Maurer, G. and Porenta, G.: artificial neural networks and spatial temporal contour linking for automated endocardial contour detection on echocardiograms: a novel approach to determine left ventricular contractile function, 1069

bioeffects
a comparison of shock wave and sinusoidal-focused ultrasound-induced localized transfection of HeLa cells (Huber), 1451
acoustic radiation force *in vivo*: a mechanism to assist targeting of microbubbles (Dayton), 1195
acoustic saturation and output regulation (Duck), 1009
angular directivity of thermal coagulation using air-cooled direct-coupled interstitial ultrasound applicators (Deardorff), 609
cell damage by lithotripter shock waves at high pressure to preclude cavitation (Williams), 1445
effect of high-intensity focused ultrasound on whole blood with and without microbubble contrast agent (Poliachik), 991
effect of macroscopic air bubbles on cell lysis by shock wave lithotripsy *in vitro* (Williams), 473
elastographic characterization of HIFU-induced lesions in canine livers (Righetti), 1099

enhancement of ultrasound-accelerated thrombolysis by echo contrast agents: dependence on microbubble structure (Mizushige), 1431
erosion of artificial endothelia *in vitro* by pulsed ultrasound: acoustic pressure, frequency, membrane orientation and microbubble contrast agent dependence (Brayman), 1305
heating vs. cavitation in the induction of mouse hindlimb paralysis by ultrasound (Miller), 1145
hemorrhage in murine fetuses exposed to pulsed ultrasound (Dalecki), 1139
histological study of normal and tumor-bearing liver treated with focused ultrasound (Chen), 847
in vitro heating of human fetal vertebra by pulsed diagnostic ultrasound (Doody), 1289
in vivo demonstration of noninvasive thermal surgery of the liver and kidney using an ultrasonic phased array (Daum), 1087
low-frequency, low-intensity ultrasound accelerates thrombolysis through the skull (Behrens), 269
sonochemically induced radicals generated by pulsed high-energy ultrasound *in vitro* and *in vivo* (Debus), 301
sonolysis of Albunex®-supplemented, 40% hematocrit human erythrocytes by pulsed 1-MHz ultrasound: pulse number, pulse duration and exposure vessel rotation dependence (Brayman), 307
sonoporation of cultured cells in the rotating tube exposure system (Miller), 143
the effect of low-frequency ultrasound on immersed pig lungs (Shupak), 1439
transient poration and cell surface receptor removal from human lymphocytes *in vitro* by 1 MHz ultrasound (Brayman), 999
ultrasonic enhancement of gene transfection in murine melanoma tumors (Miller), 1425
ultrasound power deposition model for the chest wall (Moros), 1275
ultrasound-induced cavitation damage to external epithelia of fish skin (Frenkel), 1295

Björklund, N., see Kulbisky, G. P.
Bland, P. H., see Meyer, C. R.
Bland, P. H., see Meyer, C. R.
Bloch, S., see Poliachik, S. L.
Blomley, M. J. K., Albrecht, T., Cosgrove, D. O., Eckersley, R. J., Butler-Barnes, J., Jayaram, V., Patel, N., Heckemann, R. A., Bauer, A. and Schlief, R.: stimulated acoustic emission to image a late liver and spleen-specific phase of Levovist® in mormal volunteers and patients with and without liver disease, 1341

blood
on the relation between aggregation, packing and the backscattered ultrasound signal for whole blood (Lim), 1395
the effect of hemodynamics, vessel wall compliance and hematocrit on ultrasonic Doppler power: an *in vitro* study (Missaridis), 549
ultrasonic backscattering from porcine whole blood of varying hematocrit and shear rate under pulsatile flow (Lin), 1151

blood flow
a comparison of single- and dual-beam methods for maximum velocity estimation (Hoskins), 583

a validation study on the intraobserver and interobserver reproducibility of renal artery duplex ultrasound (Baumgartner), 225
accuracy of the main Doppler methods for evaluating the degree of carotid stenoses (continuous wave, pulsed wave, and color Doppler), (Arbeille), 65
artificial neural network analysis of common femoral artery Doppler shift signals: classification of proximal disease (Wright), 735
cerebral arteriovenous transmit time (CTT): a sonographic assessment of cerebral microcirculation using ultrasound contrast agents (Puls), 503
color Doppler velocity accuracy proximal to regurgitant orifices: influence of orifice aspect ratio (Myers), 771
comparison of transcranial Doppler flow velocity and cerebral blood flow during focal ischemia in rabbits (Els), 933
effect of acquisition rate on liver and portal vein enhancement with microbubble contrast (Sirlin), 331
effect of catheter placement on 3-D velocity profiles in curved tubes resembling the human coronary system (Krams), 803
implementation of spectral width Doppler in pulsatile flow measurements (Lee), 1221
in vivo kinetics of microbubbles of SH U 508 A (Levovist®): comparison with Indocyanine Green in rabbits (Uchimoto), 1365
increased accuracy of echocardiographic measurement of flow using automated spherical integration of multiple plane velocity vectors (Brandberg), 249
intraoperative changes of transcranial Doppler velocity: relation to arterial oxygen content and whole-blood viscosity (Schuurman), 151
kinetic study of tumor blood flow in prostatic cancer using power Doppler imaging (Okihara), 89
liquid jets, accelerated thrombolysis: a study for revascularization of cerebral embolism (Kodama), 977
measurement accuracy of the flow velocity in pulsed ultrasound Doppler velocimeter (Kagiyama), 1265
middle cerebral artery anatomy and characteristics of embolic signals: a dual gate computer simulation study (Mess), 531
portal venous volume flow: *in vivo* measurement by time-domain color-velocity imaging (Kawasaki), 915
quantitative Doppler measures in coiled vessels: investigation on excised umbilical veins (Guiot), 1465
relationship of thyroid blood flow to reproductive events in normal Chinese females (Chan), 233
review of the assessment of single level and multilevel arterial occlusive disease in lower limbs by duplex ultrasound (Allard), 495
sensitivity of color Doppler sonography: an experimental approach (Delorme), 541
signal from hepatic hemangiomas on power Doppler US: real or artefactual? (Kim), 1055
the progression of thrombus in an *ex-vivo* shunt model evaluated by intravascular ultrasound radiofrequency analysis (Komiyama), 561
time-averaged mean velocity for volumetric blood flow measurements: an *in vitro* model validation study using physiological femoral artery flow waveforms (Walker), 577
transvaginal color Doppler for predicting pathological response to preoperative chemoradiation in locally advanced cervical carcinoma: a preliminary study (Alcázar), 1041

ultrasonic backscattering from porcine whole blood of varying hematocrit and shear rate under pulsatile flow (Lin), 1151
umbilical arterial blood flow in the mouse embryo during development and following acutely increased heart rate (MacLennan), 361

blood vessels
2-D and 3-D endoluminal ultrasound: vascular and nonvascular applications (Liu), 159
3-D power Doppler cerebral angiography in neonates and young infants: comparison with 2-D power Doppler angiography (Peng), 947
accuracy of the main Doppler methods for evaluating the degree of carotid stenoses (continuous wave, pulsed wave, and color Doppler), (Arbeille), 65
artificial neural network analysis of common femoral artery Doppler shift signals: classification of proximal disease (Wright), 735
carotid arterial stiffness as a surrogate for aortic stiffness: relationship between carotid artery pressure-strain elastic modulus and aortic pulse wave velocity (Nagai), 181
effect of acquisition rate on liver and portal vein enhancement with microbubble contrast (Sirlin), 331
evaluation of off-line automated intima-media thickness detection of the common carotid artery - based on M-line signal processing (Willekes), 57
experimental and clinical validation of arterial diameter waveform and intimal media thickness obtained from B-mode ultrasound image processing (Graf), 1353
hemostasis of punctured vessels using Doppler-guided high-intensity ultrasound (Martin), 985
modeling geometric artefacts in intravascular ultrasound imaging (Delachartre), 567
quantitative Doppler measures in coiled vessels: investigation on excised umbilical veins (Guiot), 1465
review of the assessment of single level and multilevel arterial occlusive disease in lower limbs by duplex ultrasound (Allard), 495
the progression of thrombus in an *ex-vivo* shunt model evaluated by intravascular ultrasound radiofrequency analysis (Komiyama), 561
three months use of third-generation oral contraceptives does not affect artery wall properties (Willekes), 723

blood viscosity
intraoperative changes of transcranial Doppler velocity: relation to arterial oxygen content and whole-blood viscosity (Schuurman), 151
the effect of hemodynamics, vessel wall compliance and hematocrit on ultrasonic Doppler power: an *in vitro* study (Missaridis), 549

Boes, J. L., see Meyer, C. R.
Bolondi, L., see Piscaglia, F.
Bom, N., see Bouakaz, A.
Bond, A. D., see Shaw, A.

bone
computational methods for ultrasonic bone assessment ((Luo), 823
on the ultrasonic attenuation and its frequency dependence in the Os Calcis assessed with a multielement receiver (Strelitzki), 133

ultrasonic propagation in cancellous bone: a new stratified model (Hughes), 811

book reviews
abdominal ultrasound principles and techniques (Freeman), 315
an atlas of neonatal brain sonography (Stringfellow), 319
cardiac ultrasound (Wilde), 317
contrast ultrasound for the radiologist (Dawson), 316
diagnostic ultrasound (Dewbury), 863
diagnostic ultrasound of fetal anomalies (in compact disk) (Smith), 1475
guidelines and gamuts in musculoskeletal ultrasound (King), 1019
obstetric ultrasound: principles and techniques (Dubbins), 316
ophthalmic ultrasound: a diagnostic atlas (Trier), 1159
ultrasonic instruments and devices – I (Preston), 491
ultrasound teaching manual: the basics of performing and interpreting ultrasound scans (Edie), 863
vascular diagnosis with ultrasound (Oates), 487

Borst, C., see Smits, P. C.
Bos, L. J., Piek, J. J., Vergroesen, I. and Spaan, J. A. E.: confounding effects of myocardial background intensity and attenuation in contrast echocardiography: an *in vivo* study, 1177
Bots, M. L., see Willekes, C.
Bouakaz, A., Frinking, P. J. A., de Jong, N. and Bom, N.: noninvasive measurement of the hydrostatic pressure in a fluid-filled cavity based on the disappearance time of micrometer-sized free gas bubbles, 1407
Bouin-Pineau, M.-H., see Arbeille, P.

boundary detection
application of a semiautomatic boundary detection algorithm for the assessment of amniotic fluid quantity from ultrasound images (Sagiv), 515
artificial neural networks and spatial temporal contour linking for automated endocardial contour detection on echocardiograms: a novel approach to determine left ventricular contractile function (Binder), 1069

bowel
contrast ultrasonography of the normal small bowel (Pallotta), 1335

brain
quantitative ultrasonography of the perventricular white and grey matter of the developing brain (Mullaart), 527

Bramley, J., see Allott, C. P.
Brandberg, J., Janerot-Sjöberg, B. and Ask, P.: increased accuracy of echocardiographic measurement of flow using automated spherical integration of multiple plane velocity vectors, 249
Brandenburger, G. H., see Marsh, J. N.
Brandenburger, G., see Dayton, P.
Brands, P. J., see Willekes, C.
Brautigam, M., see Uchimoto, R.
Brayman, A. A. and Miller, M. W.: sonolysis of Albunex®-supplemented, 40% hematocrit human erythrocytes by pulsed 1-MHz ultrasound: pulse number, pulse duration and exposure vessel rotation dependence, 307
Brayman, A. A., Coppage, M. L., Vaidya, S. and Miller, W. W.: transient

poration and cell surface receptor removal from human lymphocytes *in vitro* by 1 MHz ultrasound, 999
Brayman, A. A., Lizotte, L. M. and Miller, M. W.: erosion of artificial endothelia *in vitro* by pulsed ultrasound: acoustic pressure, frequency, membrane orientation and microbubble contrast agent dependence, 1305

breast
the use of acoustic streaming in breast lesion diagnosis: a clinical study (Nightingale), 75

Brode, S. E., see Ren, J.-F.
Brook, F., see Chan, S.-T.
Brook, F., see Ying, M.
Brown, B, see Chan, S.-T.
Brown, B., see Ying, M.
Brown, J. M., Chaloupka, J., Taylor, K. J. W., Quedens-Case, C., Alderman, J. and Greener, Y.: contrast-enhanced ultrasound for guidance of local tumor ablation, 1213

bubbles
acoustic radiation force *in vivo*: a mechanism to assist targeting of microbubbles (Dayton), 1195
broadband measurement of the scattering-to-attenuation ratio for Albunex® at 37°C (Marsh), 1321 (Technical Note)
cerebral arteriovenous transmit time (CTT): a sonographic assessment of cerebral microcirculation using ultrasound contrast agents (Puls), 503
confounding effects of myocardial background intensity and attenuation in contrast echocardiography: an *in vivo* study (Bos), 1177
effect of acquisition rate on liver and portal vein enhancement with microbubble contrast (Sirlin), 331
effect of filling gases on the backscatter from contrast microbubbles: theory and *in vivo* measurements (Forsberg), 1203
effect of high-intensity focused ultrasound on whole blood with and without microbubble contrast agent (Poliachik), 991
effect of macroscopic air bubbles on cell lysis by shock wave lithotripsy *in vitro* (Williams), 473
in vivo kinetics of microbubbles of SH U 508 A (Levovist®): comparison with Indocyanine Green in rabbits (Uchimoto), 1365
noninvasive cerebrospinal fluid shunt flow measurement by Doppler ultrasound using ultrasonically excited bubbles: a feasibility study (Lam), 371
noninvasive measurement of the hydrostatic pressure in a fluid-filled cavity based on the disappearance time of micrometer-sized free gas bubbles (Bouakaz), 1407
persistent opacification of the left ventricle and myocardium with a new echo contrast agent (Strauss), 763
pressure dependence of subharmonic signals from contrast microbubbles (Shi), 275
sonolysis of Albunex®-supplemented, 40% hematocrit human erythrocytes by pulsed 1-MHz ultrasound: pulse number, pulse duration and exposure vessel rotation dependence (Brayman), 307
sonoporation of cultured cells in the rotating tube exposure system (Miller), 143

Bude, R. O., see Tuthill, T. A.
Butler-Barnes, J., see Blomley, M. J. K.
Buyruk, H. M., see Holland, W. P. J.

C

Cachard, C., see Delachartre, P.
Callans, D. J., see Ren, J.-F.
Caps, M., see Takayama, K.
Carlier, S., see Krams, R.
Carlier, S., see Li, W.
Carson, P. L., see Meyer, C. R.
Carter, S., see Takayama, K.

catheter scanners
2-D and 3-D endoluminal ultrasound: vascular and nonvascular applications (Liu), 159
effect of catheter placement on 3-D velocity profiles in curved tubes resembling the human coronary system (Krams), 803
fetal transesophageal echocardiography utilizing a 10-F, 10-MHz intravascular ultrasound catheter – comparison with conventional maternal transabdominal fetal echocardiography in sheep (Kohl), 939
intracardiac echocardiography (9 MHz) in humans: methods, imaging views and clinical utility (Ren), 1077
modeling geometric artefacts in intravascular ultrasound imaging (Delachartre), 567
the progression of thrombus in an *ex-vivo* shunt model evaluated by intravascular ultrasound radiofrequency analysis (Komiyama), 561

carotid artery
accuracy of the main Doppler methods for evaluating the degree of carotid stenoses (continuous wave, pulsed wave, and color Doppler), (Arbeille), 65
an *in vivo* evaluation of the reproducibility of intima-media thickness measurements of the carotid artery segments using B-mode ultrasound (Montauban van Swijndregt), 323
assessment of coronary stenoses by Doppler wires: a validation study using *in vitro* modeling and computer simulations (Porenta), 793
decay index: a new carotid Doppler waveform measure associated with the Windkessel function of elastic arteries (Nagai), 1371
evaluation of off-line automated intima-media thickness detection of the common carotid artery - based on M-line signal processing (Willekes), 57
experimental and clinical validation of arterial diameter waveform and intimal media thickness obtained from B-mode ultrasound image processing (Graf), 1353
noninvasive 3-D ultrasound of atherosclerotic plaques in the Watanabe rabbit (Allott), 905

cavitation
cell damage by lithotripter shock waves at high pressure to preclude cavitation (Williams), 1445
characterization of cavitational activity in lithotripsy fields using a robust electromagnetic probe (Pye), 451

effect of high-intensity focused ultrasound on whole blood with and without microbubble contrast agent (Poliachik), 991
effect of macroscopic air bubbles on cell lysis by shock wave lithotripsy *in vitro* (Williams), 473
heating vs. cavitation in the induction of mouse hindlimb paralysis by ultrasound (Miller), 1145
rationale and derivation of MI and TI – a review (Abbott), 431
sonochemically induced radicals generated by pulsed high-energy ultrasound *in vitro* and *in vivo* (Debus), 301
ultrasound-induced cavitation damage to external epithelia of fish skin (Frenkel), 1295

cell damage
cell damage by lithotripter shock waves at high pressure to preclude cavitation (Williams), 1445
effect of high-intensity focused ultrasound on whole blood with and without microbubble contrast agent (Poliachik), 991
effect of macroscopic air bubbles on cell lysis by shock wave lithotripsy *in vitro* (Williams), 473
enhancement of ultrasound-accelerated thrombolysis by echo contrast agents: dependence on microbubble structure (Mizushige), 1431
erosion of artificial endothelia *in vitro* by pulsed ultrasound: acoustic pressure, frequency, membrane orientation and microbubble contrast agent dependence (Brayman), 1305
in vitro heating of human fetal vertebra by pulsed diagnostic ultrasound (Doody), 1289
in vivo demonstration of noninvasive thermal surgery of the liver and kidney using an ultrasonic phased array (Daum), 1087
low-frequency, low-intensity ultrasound accelerates thrombolysis through the skull (Behrens), 269
sonolysis of Albunex®-supplemented, 40% hematocrit human erythrocytes by pulsed 1-MHz ultrasound: pulse number, pulse duration and exposure vessel rotation dependence (Brayman), 307
sonoporation of cultured cells in the rotating tube exposure system (Miller), 143
the effect of low-frequency ultrasound on immersed pig lungs (Shupak), 1439
transient poration and cell surface receptor removal from human lymphocytes *in vitro* by 1 MHz ultrasound (Brayman), 999
ultrasonic enhancement of gene transfection in murine melanoma tumors (Miller), 1425
ultrasound-induced cavitation damage to external epithelia of fish skin (Frenkel), 1295

cerebral flow
cerebral arteriovenous transmit time (CTT): a sonographic assessment of cerebral microcirculation using ultrasound contrast agents (Puls), 503
comparison of transcranial Doppler flow velocity and cerebral blood flow during focal ischemia in rabbits (Els), 933
intraoperative changes of transcranial Doppler velocity: relation to arterial oxygen content and whole-blood viscosity (Schuurman), 151
liquid jets, accelerated thrombolysis: a study for revascularization of cerebral embolism (Kodama), 977

middle cerebral artery anatomy and characteristics of embolic signals: a dual gate computer simulation study (Mess), 531

cerebral emboli
bilateral cerebral emboli monitoring during extracorporeal circulation (Müllges), 755
liquid jets, accelerated thrombolysis: a study for revascularization of cerebral embolism (Kodama), 977
low-frequency, low-intensity ultrasound accelerates thrombolysis through the skull (Behrens), 269

cerebral ventricles
3-D ultrasound quantification of neonatal cerebral ventricles in different head positions (Nagdyman), 895

cervical lymphadenopathy
nodal shape (S/L) and its combination with size for assessment of cervical lymphadenopathy: which cut-off should be used? (Ying), 1169

cerebrospinal fluid flow
noninvasive cerebrospinal fluid shunt flow measurement by Doppler ultrasound using ultrasonically excited bubbles: a feasibility study (Lam), 371

Cespedes, I., see Krams, R.
Céspedes, I., see Li, W.
Chaloupka, J., see Brown, J. M.
Chambless, L. E., see Arnett, D. K.
Chan, S.-T., Brook, F., Ahuja, A., Brown, B, and Metreweli, C.: relationship of thyroid blood flow to reproductive events in normal Chinese females, 233
Chandler, W. L., see Poliachik, S. L.
Chen, L., ter Haar, G., Robertson, D., Bensted, J. P. M. and Hill, C. R.: histological study of normal and tumor-bearing liver treated with focused ultrasound, 847
Chiabrera, A., see Luo, G.
Chiang, H. K., see Lee, B.-R.
Child, S. Z., see Dalecki, D.
Choi, B. I., see Kim, T. K.
Chou, Y.-H., see Lee, B.-R.
Chronos, N. A. F., see Komiyama, N.
Clarke, R. L. and ter Haar, G. R.: production harmonics *in vitro* by high-intensity focused ultrasound, 1417
Cleveland, R. O., see Williams, J. C. Jr.
Cleveland, R.O., see Poliachik, S. L.
Cloutier, G., see Allard, L.

CNS
3-D ultrasound quantification of neonatal cerebral ventricles in different head positions (Nagdyman), 895

Coakley, W.T., see Thomas, N. E.
Cobbold, R. S. C., see Lam, K. W.
Cobbold, R. S. C., see Lim, B.
Colmenares, K., see Williams, J. C. Jr.

colour Doppler
a rotating torus phantom for assessing color Doppler accuracy (Stewart), 1251
color Doppler velocity accuracy proximal to regurgitant orifices: influence of orifice aspect ratio (Myers), 771
sensitivity of color Doppler sonography: an experimental approach (Delorme), 541
transvaginal color Doppler for predicting pathological response to preoperative chemoradiation in locally advanced cervical carcinoma: a preliminary study (Alcázar), 1041

contour detection
application of a semiautomatic boundary detection algorithm for the assessment of amniotic fluid quantity from ultrasound images (Sagiv), 515
artificial neural networks and spatial temporal contour linking for automated endocardial contour detection on echocardiograms: a novel approach to determine left ventricular contractile function (Binder), 1069

contrast agent
acoustic radiation force *in vivo*: a mechanism to assist targeting of microbubbles (Dayton), 1195
analysis of flash echo from contrast agent for designing optimal ultrasound diagnostic systems (Kamiyama), 411
broadband measurement of the scattering-to-attenuation ratio for Albunex® at 37°C (Marsh), 1321 (Technical Note)
cerebral arteriovenous transmit time (CTT): a sonographic assessment of cerebral microcirculation using ultrasound contrast agents (Puls), 503
confounding effects of myocardial background intensity and attenuation in contrast echocardiography: an *in vivo* study (Bos), 1177
contrast ultrasonography of the normal small bowel (Pallotta), 1335
contrast-enhanced ultrasound for guidance of local tumor ablation (Brown), 1213
effect of acquisition rate on liver and portal vein enhancement with microbubble contrast (Sirlin), 331
effect of ECHO contrast media on the visualization of transverse sinus thrombosis with transcranial 3-D duplex sonography (Delcker), 1063
effect of filling gases on the backscatter from contrast microbubbles: theory and *in vivo* measurements (Forsberg), 1203
effect of high-intensity focused ultrasound on whole blood with and without microbubble contrast agent (Poliachik), 991
effect of macroscopic air bubbles on cell lysis by shock wave lithotripsy *in vitro* (Williams), 473
enhancement of ultrasound-accelerated thrombolysis by echo contrast agents: dependence on microbubble structure (Mizushige), 1431
erosion of artificial endothelia *in vitro* by pulsed ultrasound: acoustic pressure, frequency, membrane orientation and microbubble contrast agent dependence (Brayman), 1305
in vivo kinetics of microbubbles of SH U 508 A (Levovist®): comparison with Indocyanine Green in rabbits (Uchimoto), 1365
noninvasive cerebrospinal fluid shunt flow measurement by Doppler ultrasound using ultrasonically excited bubbles: a feasibility study (Lam), 371
noninvasive measurement of the hydrostatic pressure in a fluid-filled cavity based on the disappearance time of micrometer-sized free gas bubbles (Bouakaz), 1407

persistent opacification of the left ventricle and myocardium with a new echo contrast agent (Strauss), 763
pressure dependence of subharmonic signals from contrast microbubbles (Shi), 275
sonolysis of Albunex®-supplemented, 40% hematocrit human erythrocytes by pulsed 1-MHz ultrasound: pulse number, pulse duration and exposure vessel rotation dependence (Brayman), 307
sonoporation of cultured cells in the rotating tube exposure system (Miller), 143
stimulated acoustic emission to image a late liver and spleen-specific phase of Levovist® in normal volunteers and patients with and without liver disease (Blomley), 1341

Coppage, M. L., see Brayman, A. A.
Corazziari, E., see Pallotta, N.

coronary artery
clinical implications of online and off-line interobserver variability in intracoronary ultrasound-guided interventions (Smits), 509
effect of catheter placement on 3-D velocity profiles in curved tubes resembling the human coronary system (Krams), 803

Cosgrove, D. O., see Blomley, M. J. K.
Cox, C., see Dalecki, D.
Creim, J. A., see Miller, D. L.
Crum, L. A., see Poliachik, S. L.
Crum, L. A., see Williams, J. C. Jr.
Crum, L., see Takayama, K.

D

D-Dimer
does venous microemboli detection add to the interpretation of D-dimer values following orthopedic surgery?, (Abraham) 637 (Clinical Note)

D'hooge, J. D., see Bijnens, B.
Daffertshofer, M., see Behrens, S.
Daffertshofer, M., see Els, T.
Dalecki, D., Child, S. Z., Raeman, C. H. and Cox, C.: hemorrhage in murine fetuses exposed to pulsed ultrasound, 1139
Daum, D. R., Smith, N. B., King, R. and Hynynen, K.: *in vivo* demonstration of noninvasive thermal surgery of the liver and kidney using an ultrasonic phased array, 1087
Davidson, F., see Ramnarine, K. V.
Dawson, P.: contrast ultrasound for the radiologist, 316 (Book Review)
Dayton, P., Klibanov, A., Brandenburger, G. and Ferrara, K.: acoustic radiation force *in vivo*: a mechanism to assist targeting of microbubbles, 1195
De Groot, E., see Montauban van Swijndregt, A. D.
de Jaegere, P. P. T., see Smits, P. C.
de Jong, N., see Bouakaz, A.
De Lange, E. E., see Montauban van Swijndregt, A. D.
Deardorff, D. L. and Diederich, C. J.: angular directivity of thermal coagulation using air-cooled direct-coupled interstitial ultrasound applicators, 609
Debus, J., Spoo, J., Jenne, J., Huber, P. and Peschke, P.: sonochemically

induced radicals generated by pulsed high-energy ultrtasound in vitro and in vivo, 301
Debus, J., see Huber, P. E.

decay index
decay index: a new carotid Doppler waveform measure associated with the Windkessel function of elastic arteries (Nagai), 1371

decorrelation
echo decorrelation estimated from signal powers (Li), 405

Deiranieh, L. H., see Sirlin, C. B.
Delachartre, P., Cachard, C., Finet, G., Gerfault, L. and Vray, D.: modeling geometric artefacts in intravascular ultrasound imaging, 567
Delcker, A., Häussermann, P. and Weimar, C.: effect of ECHO contrast media on the visualization of transverse sinus thrombosis with transcranial 3-D duplex sonography, 1063
Delorme, S., Peschke, P., Zuna, I. and Van Kaick, G.: sensitivity of color Doppler sonography: an experimental approach, 541

denoising
spectrogram enhancement algorithm: a soft thresholding-based approach (Liu), 839

Devaraju, V., see Lewin, P. A.
Dewbury, K.: diagnostic ultrasound, 863 (Book Review)
Diederich, C. J. and Hynynen, K.: ultrasound technology for hyperthermia, 871 (Review Article)
Diederich, C. J., see Deardorff, D. L.
Dineley, J. A., see Pye, S. D.
Doblar, D. D., see Mignault, K.
Donati, G., see Piscaglia, F.
Dong, F., Madsen, E. L., MacDonald, M. C. and Zagzebski, J. A.: nonlinearity parameter for tissue-mimicking materials, 831
Doody, C., Porter, H., Duck, F. A. and Humphrey, V. F.: *in vitro* heating of human fetal vertebra by pulsed diagnostic ultrasound, 1289

Doppler
3-D power Doppler cerebral angiography in neonates and young infants: comparison with 2-D power Doppler angiography (Peng), 947
a comparison of single- and dual-beam methods for maximum velocity estimation (Hoskins), 583
a rotating torus phantom for assessing color Doppler accuracy (Stewart), 1251
accuracy of the main Doppler methods for evaluating the degree of carotid stenoses (continuous wave, pulsed wave, and color Doppler), (Arbeille), 65
artificial neural network analysis of common femoral artery Doppler shift signals: classification of proximal disease (Wright), 735
assessment of coronary stenoses by Doppler wires: a validation study using *in vitro* modeling and computer simulations (Porenta), 793
bilateral cerebral emboli monitoring during extracorporeal circulation (Müllges), 755
color Doppler velocity accuracy proximal to regurgitant orifices: influence of orifice aspect ratio (Myers), 771

comparison of transcranial Doppler flow velocity and cerebral blood flow during focal ischemia in rabbits (Els), 933
decay index: a new carotid Doppler waveform measure associated with the Windkessel function of elastic arteries (Nagai), 1371
dependence of power Doppler image on a high pass filter instrumented in ultrasound machine (Mizushige), 1389
design considerations for a transcranial Doppler coupled to a stereotactic position arm (Mignault), 111
Doppler backscatter properties of a blood-mimicking fluid for Doppler performance assessment (Ramnarine), 105
Doppler evaluation of othe effects of pharmacological treatment of portal hypertension (Piscaglia), 923
effect of catheter placement on 3-D velocity profiles in curved tubes resembling the human coronary system (Krams), 803
finite beam-width ray model for geometric spectral broadening (Hoskins), 391
hemostasis of punctured vessels using Doppler-guided high-intensity ultrasound (Martin), 985
implementation of spectral width Doppler in pulsatile flow measurements (Lee), 1221
in vivo kinetics of microbubbles of SH U 508 A (Levovist®): comparison with Indocyanine Green in rabbits (Uchimoto), 1365
intraoperative changes of transcranial Doppler velocity: relation to arterial oxygen content and whole-blood viscosity (Schuurman), 151
kinetic study of tumor blood flow in prostatic cancer using power Doppler imaging (Okihara), 89
measurement accuracy of the flow velocity in pulsed ultrasound Doppler velocimeter (Kagiyama), 1265
middle cerebral artery anatomy and characteristics of embolic signals: a dual gate computer simulation study (Mess), 531
noninvasive cerebrospinal fluid shunt flow measurement by Doppler ultrasound using ultrasonically excited bubbles: a feasibility study (Lam), 371
quantitative Doppler measures in coiled vessels: investigation on excised umbilical veins (Guiot), 1465
review of the assessment of single level and multilevel arterial occlusive disease in lower limbs by duplex ultrasound (Allard), 495
sensitivity of color Doppler sonography: an experimental approach (Delorme), 541
signal from hepatic hemangiomas on power Doppler US: real or artefactual? (Kim), 1055
spectrogram analysis of arterial Doppler signals for off-line automated hits detection (Roy), 349
spectrogram enhancement algorithm: a soft thresholding-based approach (Liu), 839
tendon displacement assessment by pulsed Doppler tissue imaging: validation with a reciprocating string test target (Holland), 1229
the effect of hemodynamics, vessel wall compliance and hematocrit on ultrasonic Doppler power: an *in vitro* study (Missaridis), 549
the use of the wavelet transform to describe embolic signals (Aydin), 953
time-averaged mean velocity for volumetric blood flow measurements: an *in vitro* model validation study using physiological femoral artery flow waveforms (Walker), 577
transvaginal color Doppler for predicting pathological response to preoper-

ative chemoradiation in locally advanced cervical carcinoma: a preliminary study (Alcázar), 1041

Doukas, A. G., see Maznev, A. A.
Drake, J. M., see Lam, K. W.
Dubbins, P. A.: obstetric ultrasound: principles and techniques, 316 (Book Review)
Duck, F. A.: acoustic saturation and output regulation, 1009
Duck, F. A., see Doody, C.
Durand, L.-G., see Allard, L.

E

Earley, C. J., see Nagai, Y.
Earley, C. J., see Nagai, Y.

echo decorrelation
echo decorrelation estimated from signal powers (Li), 405

echo texture
frequency analysis of echo texture in tendon (Tuthill), 959

echocardiography
artificial neural networks and spatial temporal contour linking for automated endocardial contour detection on echocardiograms: a novel approach to determine left ventricular contractile function (Binder), 1069
confounding effects of myocardial background intensity and attenuation in contrast echocardiography: an *in vivo* study (Bos), 1177
dynamic three-dimensional freehand echocardiography using raw digital ultrasound data (Berg), 745
fetal transesophageal echocardiography utilizing a 10-F, 10-MHz intravascular ultrasound catheter – comparison with conventional maternal transabdominal fetal echocardiography in sheep (Kohl), 939
increased accuracy of echocardiographic measurement of flow using automated spherical integration of multiple plane velocity vectors (Brandberg), 249
intracardiac echocardiography (9 MHz) in humans: methods, imaging views and clinical utility (Ren), 1077
morphological evaluation of a regurgitant orifice by 3-D echocardiography: applications in the quantification of valvular regurgitation (Anayiotos), 209
persistent opacification of the left ventricle and myocardium with a new echo contrast agent (Strauss), 763

Eckersley, R. J., see Blomley, M. J. K.
Eder, V., see Tranquart, F.
Edie, J.: ultrasound teaching manual: the basics of performing and interpreting ultrasound scans, 863 (Book Review)
Eefting, F. D., see Smits, P. C.
Eguchi, H., see Uchimoto, R.
Eik-Nes, S. H., see Salvesen, K. Å.

elastic modulus
carotid arterial stiffness as a surrogate for aortic stiffness: relationship between carotid artery pressure-strain elastic modulus and aortic pulse wave velocity (Nagai), 181

decay index: a new carotid Doppler waveform measure associated with the Windkessel function of elastic arteries (Nagai), 1371
elastographic characterization of HIFU-induced lesions in canine livers (Righetti), 1099
noninvasive assessment of the viscoelasticity of peripheral arteries (Shau), 1377
three months use of third-generation oral contraceptives does not affect artery wall properties (Willekes), 723
variability in ultrasonic measurements of arterial stiffness in the atherosclerosis risk in communities study (Arnett), 175

elastography
elastographic characterization of HIFU-induced lesions in canine livers (Righetti), 1099
power spectral strain estimators in elastography (Konofagou), 1115
the feasibility of elastographic visualization of HIFU-induced thermal lesions in soft tissues (Kallel), 641 (Technical Note)

elasticity
noninvasive assessment of the viscoelasticity of peripheral arteries (Shau), 1377
the effect of hemodynamics, vessel wall compliance and hematocrit on ultrasonic Doppler power: an *in vitro* study (Missaridis), 549
variability in ultrasonic measurements of arterial stiffness in the atherosclerosis risk in communities study (Arnett), 175

Elmahdi, A. M., see Myers, J. G. Jr.
Els, T., Daffertshofer, M., Schroeck, H., Kuschinsky, W. and Hennerici, M.: comparison of transcranial Doppler flow velocity and cerebral blood flow during focal ischemia in rabbits, 933

emboli
bilateral cerebral emboli monitoring during extracorporeal circulation (Müllges), 755
does venous microemboli detection add to the interpretation of D-dimer values following orthopedic surgery?, (Abraham) 637 (Clinical Note)
enhancement of ultrasound-accelerated thrombolysis by echo contrast agents: dependence on microbubble structure (Mizushige), 1431
erosion of artificial endothelia *in vitro* by pulsed ultrasound: acoustic pressure, frequency, membrane orientation and microbubble contrast agent dependence (Brayman), 1305
frequency filtering improves ultrasonic embolic signal detection (Markus), 857 (Technical Note)
low-frequency, low-intensity ultrasound accelerates thrombolysis through the skull (Behrens), 269
middle cerebral artery anatomy and characteristics of embolic signals: a dual gate computer simulation study (Mess), 531
spectrogram analysis of arterial Doppler signals for off-line automated hits detection (Roy), 349
the progression of thrombus in an *ex-vivo* shunt model evaluated by intravascular ultrasound radiofrequency analysis (Komiyama), 561
the use of the wavelet transform to describe embolic signals (Aydin), 953

embryo
umbilical arterial blood flow in the mouse embryo during development and following acutely increased heart rate (MacLennan), 361

endocardium
artificial neural networks and spatial temporal contour linking for automated endocardial contour detection on echocardiograms: a novel approach to determine left ventricular contractile function (Binder), 1069

endoluminal
2-D and 3-D endoluminal ultrasound: vascular and nonvascular applications (Liu), 159
assessment of coronary stenoses by Doppler wires: a validation study using *in vitro* modeling and computer simulations (Porenta), 793
evaluation of off-line automated intima-media thickness detection of the common carotid artery - based on M-line signal processing (Willekes), 57
experimental and clinical validation of arterial diameter waveform and intimal media thickness obtained from B-mode ultrasound image processing (Graf), 1353

epidermis
ultrasound-induced cavitation damage to external epithelia of fish skin (Frenkel), 1295

Evan, A. P., see Williams, J. C. Jr.
Evan, A. P., see Williams, J. C. Jr.

extended field of view
SieScape™ images (Nock), 861 (Letter)

F

Fan, P., see Anayiotos, A. S.
Fan, P., see Myers, J. G. Jr.
Fan, X., see Moros, E. G.
Fast, D., see Mignault, K.
Fernandez, R., see Ronco, A. L.
Ferrara, K., see Dayton, P.

fetal liver
echogenicity of fetal lung and liver quantified by the grey-level histogram width (Maeda), 201
effect of acquisition rate on liver and portal vein enhancement with micro-bubble contrast (Sirlin), 331

fetal lung
echogenicity of fetal lung and liver quantified by the grey-level histogram width (Maeda), 201

fetus
echogenicity of fetal lung and liver quantified by the grey-level histogram width (Maeda), 201
effect of acquisition rate on liver and portal vein enhancement with micro-bubble contrast (Sirlin), 331
the fetal spinal canal - a three-dimensional study (Wallny), 1329

ultrasound during pregnancy and birthweight, childhood malignancies and neurological development (Salvesen), 1025 (Review Article)

Filipczynski, L., Kujawska, T., Tymkiewicz, R. and Wójcik, J.: nonlinear and linear propagation of diagnostic ultrasound pulses, 285
Filipczynski, L., Kujawska, T., Tymkiewicz, R. and Wójcik, J.: temperature elevation computed for three-layer and four-layer obstetrical tissue models in nonlinear and linear propagation cases, 865 (Erratum)
Filipczynski, L., see Wójcik, J.

filter
dependence of power Doppler image on a high pass filter instrumented in ultrasound machine (Mizushige), 1389

Fimmers, R., see Wallny, T. A.
Finch-Johnston, A. E., Gussak, H. M., Mobley, J., Holland, M. R., Petrovic, O., Pérez, J. E. and Miller, J. G.: dependence of "apparent" magnitude on the time delay of cyclic variation of myocardial backscatter, 759
Finet, G., see Delachartre, P.
Fish, P. J., see Hoskins, P. R.

fish
ultrasound-induced cavitation damage to external epithelia of fish skin (Frenkel), 1295

Fitzgerald, P. J., see Komiyama, N.
Fleg, J. L., see Nagai, Y.
Fleg, J. L., see Nagai, Y.
Fleming, J. E. E., see McNay, M. B.

focal ischemia
comparison of transcranial Doppler flow velocity and cerebral blood flow during focal ischemia in rabbits (Els), 933

Forsberg, F., Basude, R., Liu, J.-B., Alessandro, J., Shi, W. T., Rawool, N. M., Goldberg, B. B. and Wheatley, M. A.: effect of filling gases on the backscatter from contrast microbubbles: theory and *in vivo* measurements, 1203
Forsberg, F., see Shi, W. T.
Fowlkes, J. B., see Meyer, C. R.
Fowlkes, J. B., see Tuthill, T. A.
Freeman, S. J.: abdominal ultrasound principles and techniques, 315 (Book Review)
Frenkel, V., Kimmel, E. and Iger, Y.: ultrasound-induced cavitation damage to external epithelia of fish skin, 1295

frequency filtering
frequency filtering improves ultrasonic embolic signal detection (Markus), 857 (Technical Note)

Frinking, P. J. A., see Bouakaz, A.

G

Gaiani, S., see Piscaglia, F.
Gariepy, J., see Graf, S.

gastroduodenal function
effects of promethazine on porcine gastroduodenal function: a sonographic study (Wright), 241

Gerfault, L., see Delachartre, P.
Gies, R. A., see Miller, D. L.
Gies, R. A., see Miller, D. L.
Girard, M. S., see Sirlin, C. B.
Goldberg, B. B., see Forsberg, F.
Goldberg, B. B., see Liu, J.-B.
Goldberg, B. B., see Shi, W. T.
Gong, X.-F., see Zhang, D.
Gordon, R., see Kulbisky, G. P.
Goto, Y., see Kamiyama, N.
Gottlieb, C. D., see Ren, J.-F.
Gough, N. A. J., see Wright, I. A.
Graf, S., Gariepy, J., Massonneau, M., Armentano, R. L., Mansour, S., Barra, J. G., Simon, A. and Levenson, J.: experimental and clinical validation of arterial diameter waveform and intimal media thickness obtained from B-mode ultrasound image processing, 1353
Greener, Y., see Brown, J. M.
Grenier, N., see Tranquart, F.
Grote, C., see Berg, D.
Guiot, C., Roatta, S., Piccoli, E., Saccomandi, F. and Todros, T.: quantitative Doppler measures in coiled vessels: investigation on excised umbilical veins, 1465
Guittet, C., Ossant, F., Remenieras, J.-P., Poucelot, L. and Berson, M.: high-frequency estimation of the ultrasonic attenuation coefficient slope obtained in human skin: simulation and *in vivo* results, 421
Guo, Z., see Allard, L.
Gussak, H. M., see Finch-Johnston, A. E.
Guthrie, B., see Mignault, K.

H

ter Haar, G. R., see Clarke, R. L.
ter Haar, G., see Chen, L.
Han, J. K., see Kim, T. K.
Hansmann, M. E., see Wallny, T. A.
Hanson, S. R., see Komiyama, N.
Harker, L. A., see Komiyama, N.

harmonics
clinical use of ultrasound tissue harmonic imaging (Tranquart), 889
pressure dependence of subharmonic signals from contrast microbubbles (Shi), 275
production of harmonics *in vitro* by high-intensity focused ultrasound (Clarke), 1417

Haupt, D., see Luo, G.
Häussermann, P., see Delcker, A.
Hazle, J. D., see Kallel, F.
Hazle, J. D., see Righetti, R.
Heckemann, R. A., see Blomley, M. J. K.

Heinemeyer, O. and Reimers, C. D.: ultrasound of radial, ulnar, median, and sciatic nerves in healthy subjects and patients with hereditary motor and sensory neuropathies, 481

HELA
a comparison of shock wave and sinusoidal-focused ultrasound-induced localized transfection of HeLa cells (Huber), 1451

Helwegen, J., see Nagai, Y.

hemorrhage
hemorrhage in murine fetuses exposed to pulsed ultrasound (Dalecki), 1139

hemostasis
hemostasis of punctured vessels using Doppler-guided high-intensity ultrasound (Martin), 985

Henderson, J., see Jago, J. R.
Hennerici, M., see Behrens, S.,
Hennerici, M., see Els, T.

hepatic hemangioma
signal from hepatic hemangiomas on power Doppler US: real or artefactual? (Kim), 1055
Herault, S., see Arbeille, P.
Herregods, M.-C., see Bijnens, B.

HIFU
a comparison of shock wave and sinusoidal-focused ultrasound-induced localized transfection of HeLa cells (Huber), 1451
cell damage by lithotripter shock waves at high pressure to preclude cavitation (Williams), 1445
characterization of cavitational activity in lithotripsy fields using a robust electromagnetic probe (Pye), 451
effect of high-intensity focused ultrasound on whole blood with and without microbubble contrast agent (Poliachik), 991
effect of macroscopic air bubbles on cell lysis by shock wave lithotripsy *in vitro* (Williams), 473
elastographic characterization of HIFU-induced lesions in canine livers (Righetti), 1099
enhancement of ultrasound-accelerated thrombolysis by echo contrast agents: dependence on microbubble structure (Mizushige), 1431
erosion of artificial endothelia *in vitro* by pulsed ultrasound: acoustic pressure, frequency, membrane orientation and microbubble contrast agent dependence (Brayman), 1305
hemostasis of punctured vessels using Doppler-guided high-intensity ultrasound (Martin), 985
histological study of normal and tumor-bearing liver treated with focused ultrasound (Chen), 847
production of harmonics *in vitro* by high-intensity focused ultrasound (Clarke), 1417
the feasibility of elastographic visualization of HIFU-induced thermal lesions in soft tissues (Kallel), 641 (Technical Note)

Hill, C. R., see Chen, L.
Hirao, K., see Mizushige, K.

history
forty years of obstetric ultrasound 1957-1997: from A-scope to three dimensions (McNay), 3 (Historical Review)

Ho, Y.-L., see Liu, Y.-B.
Hoeks, A. P. G., see Willekes, C.
Hoeks, A. P. G., see Willekes, C.
Høivik, I., see Berg, S.
Holland, M. R., see Finch-Johnston, A. E.
Holland, W. P. J., Buyruk, H. M., Hoorn, E. and Stam, H. J.: tendon displacement assessment by pulsed Doppler tissue imaging: validation with a reciprocating string test target, 1229
Hoogland, H. J., see Willekes, C.
Hoorn, E., see Holland, W. P. J.
Hoskins, P. R., Fish, P. J., Pye, S. D. and Anderson, T.: finite beam-width ray model for geometric spectral broadening, 391
Hoskins, P. R.: a comparison of single- and dual-beam methods for maximum velocity estimation, 583
Hoskins, P. R., see Ramnarine, K. V.
Hsieh, F.-J., see Peng, S. S.-F.
Hsu, T.-C., see Shau, Y.-W.
Huber, P. E., Jenne, J., Debus, J., Wannenmacher, M. F. and Pfisterer, P.: a comparison of shock wave and sinusoidal-focused ultrasound-induced localized transfection of HeLa cells, 1451
Huber, P., see Debus, J.
Hubert, L., see Abraham, P.
Hughes, E. R., Leighton, T. G., Petley, G. W. and White, P. R.: ultrasonic propagation in cancellous bone: a new stratified model, 811
Hughes, M. S., see Marsh, J. N.
Humphrey, V. F., see Doody, C.

hydrophone
voltage sensitivity response of ultrasonic hydrophones in the frequency range 0.25-2.5 MHz (Lewin), 1131

hydrostatic pressure
noninvasive measurement of the hydrostatic pressure in a fluid-filled cavity based on the disappearance time of micrometer-sized free gas bubbles (Bouakaz), 1407

Hynynen, K., see Daum, D. R.
Hynynen, K., see Diederich, C. J.

hyperthermia
ultrasound technology for hyperthermia (Diederich), 871 (Review Article)

I

Iger, Y., see Frenkel, V.

image processing
application of a semiautomatic boundary detection algorithm for the assessment of amniotic fluid quantity from ultrasound images (Sagiv), 515
artificial neural networks and spatial temporal contour linking for automated endocardial contour detection on echocardiograms: a novel approach to determine left ventricular contractile function (Binder), 1069
computerized quantification of structures within ovarian cysts using ultrasound images (Zimmer), 189
evaluation of off-line automated intima-media thickness detection of the common carotid artery - based on M-line signal processing (Willekes), 57
experimental and clinical validation of arterial diameter waveform and intimal media thickness obtained from B-mode ultrasound image processing (Graf), 1353

immunoassay
ultrasonic enhancement of coated particle agglutination immunoassays: influence of particle density (Thomas), 443

iron accumulation
iron accumulation in the substantia nigra in rats visualized by ultrasound (Berg), 901

Itani, T., see Kawasaki, T.

IVUS
2-D and 3-D endoluminal ultrasound: vascular and nonvascular applications (Liu), 159
fetal transesophageal echocardiography utilizing a 10-F, 10-MHz intravascular ultrasound catheter – comparison with conventional maternal transabdominal fetal echocardiography in sheep (Kohl), 939
modeling geometric artefacts in intravascular ultrasound imaging (Delachartre), 567
the progression of thrombus in an *ex-vivo* shunt model evaluated by intravascular ultrasound radiofrequency analysis (Komiyama), 561

J

Jago, J. R., Henderson, J., Whittingham, T. A., and Mitchell, G.: a comparison of AIUM/NEMA thermal indices with calculated temperature rises for a simple third-trimester pregnancy tissue model, 623
Jamadar, D. A., see Tuthill, T. A.
Janerot-Sjöberg, B., see Brandberg, J.
Jayaram, V., see Blomley, M. J. K.
Jenne, J., see Debus, J.
Jenne, J., see Huber, P. E.
John, N. W., see Allott, C. P.
Jurado, M., see Alcázar, J. L.

K

Kaczkowski, P., see Poliachik, S. L.
Kaczkowski, P., see Takayama, K.
Kagiyama, M., Ogasawara, Y., Tadaoka, S. and Kajiya, F.: measurement accuracy of the flow velocity in pulsed ultrasound Doppler velocimeter, 1265

Kajiya, F., see Kagiyama, M.
Kallel, F., Stafford, R. J., Price, R. E., Righetti, R., Ophir, J. and Hazle, J. D.: the feasibility of elastographic visualization of HIFU-induced thermal lesions in soft tissues, 641 (Technical Note)
Kallel, F., see Righetti, R.
Kamiyama, N., Moriyasu, F., Mine, Y. and Goto, Y.: analysis of flash echo from contrast agent for designing optimal ultrasound diagnostic systems, 411
Kamiyama, N., see Uchimoto, R.
Kampmann, W., see Nagdyman, N.
Kao, H.-L., see Liu, Y.-B.
Kaufman, J. J., see Luo, G.
Kawasaki, T., Itani, T., Mimura, J. and Komori, H.: portal venous volume flow: *in vivo* measurement by time-domain color-velocity imaging, 915
Keilman, G., see Poliachik, S. L.
Keilman, G., see Takayama, K.
Keizer, H. A., see Willekes, C.
Keller, B. B., see MacLennan, M. J.
Kelly, A. B., see Komiyama, N.
Kemper, M. K., see Nagai, Y.
Kemper, M. K., see Nagai, Y.

kidney
a validation study on the intraobserver and interobserver reproducibility of renal artery duplex ultrasound (Baumgartner), 225
in vivo demonstration of noninvasive thermal surgery of the liver and kidney using an ultrasonic phased array (Daum), 1087

Kim, A. Y., see Kim, T. K.
Kim, B., see Meyer, C. R.
Kim, H., see Arnett, D. K.
Kim, T. K., Han, J. K., Kim, A. Y., Park, S. J. and Choi, B. I.: signal from hepatic hemangiomas on power Doppler US: real or artefactual?, 1055
Kimmel, E., see Frenkel, V.
King, D.: guidelines and gamuts in musculoskeletal ultrasound, 1019 (Book Review)
King, R., see Daum, D. R.
Kinoshita, A., see Masugata, H.
Klibanov, A., see Dayton, P.
Kodama, T., Tatsuno, M., Sugimoto, S., Uenohara, H., Yoshimoto, T. and Takayama, K.: liquid jets, accelerated thrombolysis: a study for revascularization of cerebral embolism, 977
Kohl, T., Suda, K., Reckers, J., Scheld, H. H., Vogt, J. and Silverman, N. H.: fetal transesophageal echocardiography utilizing a 10-F, 10-MHz intravascular ultrasound catheter – comparison with conventional maternal transabdominal fetal echocardiography in sheep, 939
Kojima, M., see Okihara, K.
Kolda, M., see Anayiotos, A. S.
Komiyama, N., Chronos, N. A. F., Uren, N. G., Moore, P., Kelly, A. B., Harker, L. A., Hanson, S. R., Metz, J. A., Yock, P. G. and Fitzgerald, P. J.: the progression of thrombus in an *ex-vivo* shunt model evaluated by intravascular ultrasound radiofrequency analysis, 561
Komori, H., see Kawasaki, T.
Kondo, I., see Mizushige, K.

Konofagou, E. E., Varghese, T., Ophir, J. and Alam, S. K.: power spectral strain estimators in elastography, 1115
Kornguth, P. J., see Nightingale, K. R.
Koyma, W., see Mihara, S.
Krams, R., Wentzel, J. J., Cespedes, I., Vinke, R., Carlier, S., van der Steen, A. F. W., Lancee, C. T. and Slager, C. J.: effect of catheter placement on 3-D velocity profiles in curved tubes resembling the human coronary system, 803
Krouskop, T. A., see Righetti, R.
Kujawska, T., see Filipczynski, L.
Kujawska, T., see Filipczynski, L.
Kujawska, T., see Wójcik, J.
Kulbisky, G. P., Rickey, D. W., Reed, M. H., Björklund, N. and Gordon, R.: the axolotl as an animal model for the comparison of 3-D ultrasound with plain film radiography, 969
Kuo, C.-D., see Lee, B.-R.
Kuo, P.-L., Li, P.-C., Shun, C.-T. and Lai, J.-S.: strain measurements of rabbit Achilles tendons by ultrasound, 1241
Kuroda, K., see Mihara, S.
Kuschinsky, W., see Els, T.

L

Lai, J.-S., see Kuo, P.-L.
Lam, K. W., Drake, J. M. and Cobbold, R. S. C.: noninvasive cerebrospinal fluid shunt flow measurement by Doppler ultrasound using ultrasonically excited bubbles: a feasibility study, 371
Lancee, C. T., see Krams, R.

laser ultrasound
wide-band spectroscopy of biological material based on a laser-induced grating technique (Maznev), 601

Lecarpentier, G. L., see Meyer, C. R.
Lee, B.-R., Chiang, H. K., Chou, Y.-H., Kuo, C.-D., Wang, J.-H. and Lee, S.-K.: implementation of spectral width Doppler in pulsatile flow measurements, 1221
Lee, F. T., see Lu, Z. F.
Lee, S.-K., see Lee, B.-R.
Lee, W.-T., see Peng, S. S.-F.
Lee, Y.-T., see Liu, Y.-B.

left ventricle
persistent opacification of the left ventricle and myocardium with a new echo contrast agent (Strauss), 763

Leighton, T. G., see Hughes, E. R.
Levenson, J., see Graf, S.
Lewin, P. A., Bautista, R. and Devaraju, V.: voltage sensitivity response of ultrasonic hydrophones in the frequency range 0.25-2.5 MHz, 1131
Li, P.-C., see Kuo, P.-L.
Li, W., Mastik, F., Céspedes, I., Carlier, S. and van der Steen, A. F. W.: echo decorrelation estimated from signal powers, 405
Li, Y-.W., see Peng, S. S.-F.

Lim, B. and Cobbold, R. S. C.: on the relation between aggregation, packing and the backscattered ultrasound signal for whole blood, 1395
Lin, J.-H., see Peng, S. S.-F.
Lin, L.-C., see Liu, Y.-B.
Lin, Y.-H. and Shung, K. K.: ultrasonic backscattering from porcine whole blood of varying hematocrit and shear rate under pulsatile flow, 1151
Linney, J. H., see Luo, G.

liquid jets
liquid jets, accelerated thrombolysis: a study for revascularization of cerebral embolism (Kodama), 977

lithotripsy
a comparison of shock wave and sinusoidal-focused ultrasound-induced localized transfection of HeLa cells (Huber), 1451
cell damage by lithotripter shock waves at high pressure to preclude cavitation (Williams), 1445
characterization of cavitational activity in lithotripsy fields using a robust electromagnetic probe (Pye), 451
effect of high-intensity focused ultrasound on whole blood with and without microbubble contrast agent (Poliachik), 991
effect of macroscopic air bubbles on cell lysis by shock wave lithotripsy *in vitro* (Williams), 473

Liu, B., Wang, Y. and Wang, W.: spectrogram enhancement algorithm: a soft thresholding-based approach, 839
Liu, H.-M., see Peng, S. S.-F.
Liu, J.-B. and Goldberg, B. B.: 2-D and 3-D endoluminal ultrasound: vascular and nonvascular applications, 159
Liu, J.-B., see Forsberg, F.
Liu, Y.-B., Wu, C.-C., Lin, L.-C., Ho, Y.-L., Kao, H.-L. and Lee, Y.-T.: alterations in ultrasonic backscatter during intra-aortic balloon counterpulsation support in patients with acute myocardial infarction, 1185

liver
echogenicity of fetal lung and liver quantified by the grey-level histogram width (Maeda), 201
effect of acquisition rate on liver and portal vein enhancement with microbubble contrast (Sirlin), 331
elastographic characterization of HIFU-induced lesions in canine livers (Righetti), 1099
histological study of normal and tumor-bearing liver treated with focused ultrasound (Chen), 847
in vivo demonstration of noninvasive thermal surgery of the liver and kidney using an ultrasonic phased array (Daum), 1087
stimulated acoustic emission to image a late liver and spleen-specific phase of Levovist® in normal volunteers and patients with and without liver disease (Blomley), 1341
ultrasound backscatter and attenuation in human liver with diffuse disease (Lu), 1047

Lizotte, L. M., see Brayman, A. A.
Lu, Z. F., Zagzebski, J. A. and Lee, F. T.: ultrasound backscatter and attenuation in human liver with diffuse disease, 1047

lungs
the effect of low-frequency ultrasound on immersed pig lungs (Shupak), 1439

Luo, G., Kaufman, J. J., Chiabrera, A., Bianco, B., Linney, J. H., Haupt, D., Ryaby, J. T. and Siffert, R. S.: computational methods for ultrasonic bone assessment, 823

lymphadenopathy
nodal shape (S/L) and its combination with size for assessment of cervical lymphadenopathy: which cut-off should be used? (Ying), 1169

lymphocytes
transient poration and cell surface receptor removal from human lymphocytes *in vitro* by 1 MHz ultrasound (Brayman), 999

M

MacDonald, M. C., see Dong, F.
MacLennan, M. J. and Keller, B. B.: umbilical arterial blood flow in the mouse embryo during development and following acutely increased heart rate, 361
Madsen, E. L., see Dong, F.
Maeda, K., Utsu, M., Yamamoto, N. and Serizawa, M.: echogenicity of fetal lung and liver quantified by the grey-level histogram width, 201
Mansour, S., see Graf, S.
Marchlinski, F. E., see Ren, J.-F.
Markus, H. S. and Reid, G.: frequency filtering improves ultrasonic embolic signal detection, 857 (Technical Note)
Markus, H. S., see Aydin, N.
Marsh, J. N., Hughes, M. S., Brandenburger, G. H. and Miller, J. G.: broadband measurement of the scattering-to-attenuation ratio for Albunex® at 37°C, 1321 (Technical Note)
Martens, D., see Berg, S.
Martin, R. W., Vaezy, S., Kaczkowski, P., Keilman, G., Carter, S., Caps, M., Beach, K., Plett, M. and Crum, L.: hemostasis of punctured vessels using Doppler-guided high-intensity ultrasound, 985
Masi, L., see Piscaglia, F.
Massonneau, M., see Graf, S.
Mastik, F., see Li, W.
Masugata, H., Mizushige, K., Senda, S., Kinoshita, A., Sakamoto, H., Sakamoto, S. and Matsuo, H.: relationship between myocardial tissue density measured by microgravimetry and sound speed measured by acoustic microscopy, 1459 (Clinical Note)
Matsuo, H., see Masugata, H.
Matsuo, H., see Mizushige, K.
Matsuo, H., see Mizushige, K.
Mattrey, R. F., see Sirlin, C. B.
Maurer, G., see Binder, T.
Maurer, G., see Porenta, G.
Mäurer, M., see Berg, D.
Mäurer, M., see Puls, I.
Maznev, A. A., McAuliffe, D. J., Doukas, A. G. and Nelson, K. A.: wide-band

spectroscopy of biological material based on a laser-induced grating technique, 601
McAteer, J. A., see Williams, J. C. Jr.
McAteer, J. A., see Williams, J. C. Jr.
McAuliffe, D. J., see Maznev, A. A.
McKelvey, G. M., see Wright, A. B.
McNay, M. B. and Fleming, J. E. E.: forty years of obstetric ultrasound 1957-1997: from A-scope to three dimensions, 3 (Historical Review)
Mellor, P. M., see Allott, C. P.
Mess, W. H., Titulaer, B. M. and Ackerstaff, R. G. A.: middle cerebral artery anatomy and characteristics of embolic signals: a dual gate computer simulation study, 531
Metcalfe, S. C., see Strelitzki, R.
Metreweli, C., see Chan, S.-T.
Metreweli, C., see Ying, M.
Metter, E. J., see Nagai, Y.
Metter, E. J., see Nagai, Y.
Metz, J. A., see Komiyama, N.
Meyer, C. R., Boes, J. L., Kim, B., Bland, P. H., Lecarpentier, G. L., Fowlkes, J. B., Roubidoux, M. A. and Carson, P. L.: semiautomatic registration of volumetric ultrasound scans, 339

microbubbles
acoustic radiation force *in vivo*: a mechanism to assist targeting of microbubbles (Dayton), 1195
analysis of flash echo from contrast agent for designing optimal ultrasound diagnostic systems (Kamiyama), 411
broadband measurement of the scattering-to-attenuation ratio for Albunex® at 37°C (Marsh), 1321 (Technical Note)
effect of filling gases on the backscatter from contrast microbubbles: theory and *in vivo* measurements (Forsberg), 1203
enhancement of ultrasound-accelerated thrombolysis by echo contrast agents: dependence on microbubble structure (Mizushige), 1431
erosion of artificial endothelia *in vitro* by pulsed ultrasound: acoustic pressure, frequency, membrane orientation and microbubble contrast agent dependence (Brayman), 1305
in vivo kinetics of microbubbles of SH U 508 A (Levovist®): comparison with Indocyanine Green in rabbits (Uchimoto), 1365
noninvasive cerebrospinal fluid shunt flow measurement by Doppler ultrasound using ultrasonically excited bubbles: a feasibility study (Lam), 371
noninvasive measurement of the hydrostatic pressure in a fluid-filled cavity based on the disappearance time of micrometer-sized free gas bubbles (Bouakaz), 1407
persistent opacification of the left ventricle and myocardium with a new echo contrast agent (Strauss), 763
pressure dependence of subharmonic signals from contrast microbubbles (Shi), 275
sonolysis of Albunex®-supplemented, 40% hematocrit human erythrocytes by pulsed 1-MHz ultrasound: pulse number, pulse duration and exposure vessel rotation dependence (Brayman), 307
sonoporation of cultured cells in the rotating tube exposure system (Miller), 143
stimulated acoustic emission to image a late liver and spleen-specific phase

of Levovist® in normal volunteers and patients with and without liver disease (Blomley), 1341

Mignault, K., Doblar, D. D., Guthrie, B. and Fast, D.: design considerations for a transcranial Doppler coupled to a stereotactic position arm, 111
Mihara, S., Kuroda, K., Yoshioka, R. and Koyma, W.: early detection of renal cell carcinoma by ultrasonographic screening - based on the results of 13 years screening in Japan, 1033
Miller, D. L., Bao, S. and Morris, J. E.: sonoporation of cultured cells in the rotating tube exposure system, 143
Miller, D. L., Bao, S., Gies, R. A. and Thrall, B. D.: ultrasonic enhancement of gene transfection in murine melanoma tumors, 1425
Miller, D. L., Creim, J. A. and Gies, R. A.: heating vs. cavitation in the induction of mouse hindlimb paralysis by ultrasound, 1145
Miller, J. G., see Finch-Johnston, A. E.
Miller, J. G., see Marsh, J. N.
Miller, M. W., see Brayman, A. A.
Miller, M. W., see Brayman, A. A.
Miller, W. W., see Brayman, A. A.
Mimura, J., see Kawasaki, T.
Mine, Y., see Kamiyama, N.
Mine, Y., see Uchimoto, R.
Missaridis, T. X. and Shung, K. K.: the effect of hemodynamics, vessel wall compliance and hematocrit on ultrasonic Doppler power: an *in vitro* study, 549
Mitchell, G., see Jago, J. R.
Miyazawa, T., see Uchimoto, R.
Mizushige, K., Kondo, I., Ohmori, K., Hirao, K. and Matsuo, H.: enhancement of ultrasound-accelerated thrombolysis by echo contrast agents: dependence on microbubble structure, 1431
Mizushige, K., see Masugata, H.
Mizushige, K., Ueda, T., Yuba, M., Seki, M., Ohmori, K., Nozaki, S. and Matsuo, H.: dependence of power Doppler image on a high pass filter instrumented in ultrasound machine, 1389
Mobley, J., see Finch-Johnston, A. E.

modeling
assessment of coronary stenoses by Doppler wires: a validation study using *in vitro* modeling and computer simulations (Porenta), 793
finite beam-width ray model for geometric spectral broadening (Hoskins), 391
high-frequency estimation of the ultrasonic attenuation coefficient slope obtained in human skin: simulation and *in vivo* results (Guittet), 421
modeling geometric artefacts in intravascular ultrasound imaging (Delachartre), 567
temperature elevation computed for three-layer and four-layer obstetrical tissue models in nonlinear and linear propagation cases (Filipczynski), 865 (Erratum)
temperature elevations computed for three-layer and four-layer obstetrical tissue models in nonlinear and linear ultrasonic propagation cases (Wójcik), 259
the axolotl as an animal model for the comparison of 3-D ultrasound with plain film radiography (Kulbisky), 969

the progression of thrombus in an *ex-vivo* shunt model evaluated by intravascular ultrasound radiofrequency analysis (Komiyama), 561
time-averaged mean velocity for volumetric blood flow measurements: an *in vitro* model validation study using physiological femoral artery flow waveforms (Walker), 577
ultrasonic propagation in cancellous bone: a new stratified model (Hughes), 811
ultrasound power deposition model for the chest wall (Moros), 1275

Moertl, D., see Binder, T.
Moertl, D., see Porenta, G.
Montauban van Swijndregt, A. D., De Lange, E. E., De Groot, E. and Ackerstaff, R. G. A.: an *in vivo* evaluation of the reproducibility of intima-media thickness measurements of the carotid artery segments using B-mode ultrasound, 323
Moros, E. G., Fan, X. and Straube, W. L.: ultrasound power deposition model for the chest wall, 1275
Mullaart, R. A., Thijssen, J. M., Rotteveel, J. J., Valckx, F. M. and van Geemen, A. J.: quantitative ultrasonography of the perventricular white and grey matter of the developing brain, 527
Müllges, W., Berg, D. and Toyka, K. V.: bilateral cerebral emboli monitoring during extracorporeal circulation, 755
Myers, J. G. Jr., Anayiotos, A. A., Elmahdi, A. M., Perry, G. J., Fan, P. and Nanda, N. C.: color Doppler velocity accuracy proximal to regurgitant orifices: influence of orifice aspect ratio, 771
Montrésor, S., see Roy, E.
Moore, P., see Komiyama, N.
Moriyasu, F., see Kamiyama, N.
Morris, J. E., see Miller, D. L.
Mourad, P. D., see Poliachik, S. L.

mouse
umbilical arterial blood flow in the mouse embryo during development and following acutely increased heart rate (MacLennan), 361

Müllges, W., see Puls, I.

myocardium
dependence of "apparent" magnitude on the time delay of cyclic variation of myocardial backscatter (Finch-Johnston), 759
persistent opacification of the left ventricle and myocardium with a new echo contrast agent (Strauss), 763
relationship between myocardial tissue density measured by microgravimetry and sound speed measured by acoustic microscopy (Masugata), 1459 (Clinical Note)
robustness of integrated backscatter for myocardial tissue characterization (Bijnens), 95

myocardial infarction
alterations in ultrasonic backscatter during intra-aortic balloon counterpulsation support in patients with acute myocardial infarction (Liu), 1185

N

Nagai, Y., Fleg, J. L., Kemper, M. K., Rywik, T. M., Earley, C. J. and Metter, E. J.: carotid arterial stiffness as a surrogate for aortic stiffness: relation-

ship between carotid artery pressure-strain elastic modulus and aortic pulse wave velocity, 181
Nagai, Y., Helwegen, J., Fleg, J. L., Kemper, M. K., Earley, C. J., Rywik, T. M., Wijn, P. and Metter, E. J.: decay index: a new carotid Doppler waveform measure associated with the Windkessel function of elastic arteries, 1371
Nagdyman, N., Walka, M. M., Kampmann, W., Stöver, B. and Obladen, M.: 3-D ultrasound quantification of neonatal cerebral ventricles in different head positions, 895
Nanda, N. C., see Anayiotos, A. S.
Nanda, N. C., see Myers, J. G. Jr.

native harmonic imaging
clinical use of ultrasound tissue harmonic imaging (Tranquart), 889

Needleman, L., see Shi, W. T.
Nelson, K. A., see Maznev, A. A.

neonates
3-D power Doppler cerebral angiography in neonates and young infants: comparison with 2-D power Doppler angiography (Peng), 947
3-D ultrasound quantification of neonatal cerebral ventricles in different head positions (Nagdyman), 895
ultrasound during pregnancy and birthweight, childhood malignancies and neurological development (Salvesen), 1025 (Review Article)

nerves
ultrasound of radial, ulnar, median, and sciatic nerves in healthy subjects and patients with hereditary motor and sensory neuropathies (Heinemeyer), 481

neural networks
artificial neural network analysis of common femoral artery Doppler shift signals: classification of proximal disease (Wright), 735
artificial neural networks and spatial temporal contour linking for automated endocardial contour detection on echocardiograms: a novel approach to determine left ventricular contractile function (Binder), 1069
improving ultrasonographic diagnosis of prostate cancer with neural networks (Ronco), 729

neuropathy
ultrasound of radial, ulnar, median, and sciatic nerves in healthy subjects and patients with hereditary motor and sensory neuropathies (Heinemeyer), 481

Nicholson, P. H. F., see Strelitzki, R.
Nightingale, K. R., Kornguth, P. J. and Trahey, G. E.: the use of acoustic streaming in breast lesion diagnosis: a clinical study, 75
Niwa, K., see Uchimoto, R.
Nock, L. F.: SieScape™ images, 861 (Letter)

nodes
nodal shape (S/L) and its combination with size for assessment of cervical lymphadenopathy: which cut-off should be used? (Ying), 1169

nonlinearity parameter
experimental investigation of the acoustic nonlinearity parameter tomography for excised pathological biological tissues (Zhang), 593
nonlinear and linear propagation of diagnostic ultrasound pulses (Filipczynski), 285
nonlinearity parameter for tissue-mimicking materials (Dong), 831
temperature elevation computed for three-layer and four-layer obstetrical tissue models in nonlinear and linear propagation cases (Filipczynski), 865 (Erratum)
temperature elevations computed for three-layer and four-layer obstetrical tissue models in nonlinear and linear ultrasonic propagation cases (Wójcik), 259
the use of acoustic streaming in breast lesion diagnosis: a clinical study (Nightingale), 75

Nozaki, S., see Mizushige, K.
Nuyts, J., see Bijnens, B.

O

Oates, C.P.: vascular diagnosis with ultrasound, 487 (Book Review)
Obladen, M., see Nagdyman, N.

observer
a validation study on the intraobserver and interobserver reproducibility of renal artery duplex ultrasound (Baumgartner), 225
clinical implications of online and off-line interobserver variability in intracoronary ultrasound-guided interventions (Smits), 509

obstetrics
application of a semiautomatic boundary detection algorithm for the assessment of amniotic fluid quantity from ultrasound images (Sagiv), 515
forty years of obstetric ultrasound 1957-1997: from A-scope to three dimensions (McNay), 3 (Historical Review)
temperature elevation computed for three-layer and four-layer obstetrical tissue models in nonlinear and linear propagation cases (Filipczynski), 865 (Erratum)
temperature elevations computed for three-layer and four-layer obstetrical tissue models in nonlinear and linear ultrasonic propagation cases (Wójcik), 259
ultrasound during pregnancy and birthweight, childhood malignancies and neurological development (Salvesen), 1025 (Review Article)

Ogasawara, Y., see Kagiyama, M.
Ohmori, K., see Mizushige, K.
Ohmori, K., see Mizushige, K.
Okihara, K., Watanabe, H. and Kojima, M.: kinetic study of tumor blood flow in prostatic cancer using power Doppler imaging, 89
Olstad, B., see Berg, S.
Ophir, J., see Kallel, F.
Ophir, J., see Konofagou, E. E.
Ophir, J., see Righetti, R.
Ossant, F., see Guittet, C.

ovarian cysts
computerized quantification of structures within ovarian cysts using ultrasound images (Zimmer), 189

P

Padayachee, S., see Aydin, N.
Paech, V., see Strelitzki, R.
Pallotta, N., Baccini, F. and Corazziari, E.: contrast ultrasonography of the normal small bowel, 1335
Park, S. J., see Kim, T. K.
Pasterkamp, G., see Smits, P. C.
Patel, N., see Blomley, M. J. K.
Pay, N. M., see Shaw, A.
Peng, S. S.-F., Lin, J.-H., Lee, W.-T., Tsao, P.-N., Shih, J. C., Liu, H.-M., Li, Y-.W., Hsieh, F.-J. and Tsou, K.-I. Y.: 3-D power Doppler cerebral angiography in neonates and young infants: comparison with 2-D power Doppler angiography, 947
Pentaris, A., see Porenta, G.
Pérez, J. E., see Finch-Johnston, A. E.
Perry, G. J., see Myers, J. G. Jr.
Peschke, P., see Debus, J.
Peschke, P., see Delorme, S.
Petley, G. W., see Hughes, E. R.
Petrovic, O., see Finch-Johnston, A. E.
Pfisterer, P., see Huber, P. E.

phantom
a rotating torus phantom for assessing color Doppler accuracy (Stewart), 1251
Doppler backscatter properties of a blood-mimicking fluid for Doppler performance assessment (Ramnarine), 105
nonlinearity parameter for tissue-mimicking materials (Dong), 831
proposed standard thermal test object for medical ultrasound (Shaw), 121
tendon displacement assessment by pulsed Doppler tissue imaging: validation with a reciprocating string test target (Holland), 1229

Piccoli, E., see Guiot, C.
Pidhorz, L., see Abraham, P.
Piek, J. J., see Bos, L. J.
Piscaglia, F., Gaiani, S., Donati, G., Masi, L. and Bolondi, L.: Doppler evaluation of othe effects of pharmacological treatment of portal hypertension, 923
Plett, M., see Takayama, K.
Poliachik, S. L., Chandler, W. L., Mourad, P. D., Bailey, M. R., Bloch, S., Cleveland, R.O., Kaczkowski, P., Keilman, G., Porter, T. and Crum, L. A.: effect of high-intensity focused ultrasound on whole blood with and without microbubble contrast agent, 991
Porenta, G., Schima, H., Pentaris, A., Tsangaris, S., Moertl, D., Probst, P., Maurer, G. and Baumgartner, H.: assessment of coronary stenoses by Doppler wires: a validation study using *in vitro* modeling and computer simulations, 793
Porenta, G., see Binder, T.

portal vein
Doppler evaluation of the effects of pharmacological treatment of portal hypertension (Piscaglia), 923
effect of acquisition rate on liver and portal vein enhancement with microbubble contrast (Sirlin), 331
portal venous volume flow: *in vivo* measurement by time-domain color-velocity imaging (Kawasaki), 915

Porter, H., see Doody, C.
Porter, T., see Poliachik, S. L.
Post, E. J., see Wright, A. B.
Poucelot, L., see Guittet, C.
Pourcelot, L., see Tranquart, F.

power Doppler image
dependence of power Doppler image on a high pass filter instrumented in ultrasound machine (Mizushige), 1389
kinetic study of tumor blood flow in prostatic cancer using power Doppler imaging (Okihara), 89

pregnancy
a comparison of AIUM/NEMA thermal indices with calculated temperature rises for a simple third-trimester pregnancy tissue model (Jago), 623

pressure
noninvasive measurement of the hydrostatic pressure in a fluid-filled cavity based on the disappearance time of micrometer-sized free gas bubbles (Bouakaz), 1407

Preston, R. C.: ultrasonic instruments and devices – I, 491 (Book Review)
Preston, R. C., see Shaw, A.
Price, R. E., see Kallel, F.
Price, R. E., see Righetti, R.
Probst, P., see Porenta, G.

promethazine
effects of promethazine on porcine gastroduodenal function: a sonographic study (Wright), 241

prostate cancer
improving ultrasonographic diagnosis of prostate cancer with neural networks (Ronco), 729
kinetic study of tumor blood flow in prostatic cancer using power Doppler imaging (Okihara), 89

Puls, I., Becker, G., Mäurer, M. and Müllges, W.: cerebral arteriovenous transmit time (CTT): a sonographic assessment of cerebral microcirculation using ultrasound contrast agents, 503

pulse wave velocity
carotid arterial stiffness as a surrogate for aortic stiffness: relationship between carotid artery pressure-strain elastic modulus and aortic pulse wave velocity (Nagai), 181

Pye, S. D. and Dineley, J. A.: characterization of cavitational activity in lithotripsy fields using a robust electromagnetic probe, 451
Pye, S. D., see Hoskins, P. R.

Q

quantification
3-D ultrasound quantification of neonatal cerebral ventricles in different head positions (Nagdyman), 895
accuracy of the main Doppler methods for evaluating the degree of carotid stenoses (continuous wave, pulsed wave, and color Doppler), (Arbeille), 65
an *in vivo* evaluation of the reproducibility of intima-media thickness measurements of the carotid artery segments using B-mode ultrasound (Montauban van Swijndregt), 323
analysis of flash echo from contrast agent for designing optimal ultrasound diagnostic systems (Kamiyama), 411
artificial neural network analysis of common femoral artery Doppler shift signals: classification of proximal disease (Wright), 735
computerized quantification of structures within ovarian cysts using ultrasound images (Zimmer), 189
high-frequency estimation of the ultrasonic attenuation coefficient slope obtained in human skin: simulation and *in vivo* results (Guittet), 421
measurement accuracy of the flow velocity in pulsed ultrasound Doppler velocimeter (Kagiyama), 1265
morphological evaluation of a regurgitant orifice by 3-D echocardiography: applications in the quantification of valvular regurgitation (Anayiotos), 209
quantitative Doppler measures in coiled vessels: investigation on excised umbilical veins (Guiot), 1465
quantitative ultrasonography of the perventricular white and grey matter of the developing brain (Mullaart), 527
time-averaged mean velocity for volumetric blood flow measurements: an *in vitro* model validation study using physiological femoral artery flow waveforms (Walker), 577
wide-band spectroscopy of biological material based on a laser-induced grating technique (Maznev), 601

Quedens-Case, C., see Brown, J. M.

R

radiation force
acoustic radiation force *in vivo*: a mechanism to assist targeting of microbubbles (Dayton), 1195

radicles
sonochemically induced radicals generated by pulsed high-energy ultrasound *in vitro* and *in vivo* (Debus), 301

Raeman, C. H., see Dalecki, D.
Raichlen, J. S., see Shi, W. T.
Ramnarine, K. V., Hoskins, P. R., Routh, H. F. and Davidson, F.: Doppler backscatter properties of a blood-mimicking fluid for Doppler performance assessment, 105

Rausch, W.-D., see Berg, D.
Rawool, N. M., see Forsberg, F.
Reckers, J., see Kohl, T.
Reed, M. H., see Kulbisky, G. P.
Ren, J.-F., Schwartzman, D., Callans, D. J., Brode, S. E., Gottlieb, C. D. and Marchlinski, F. E.: intracardiac echocardiography (9 MHz) in humans: methods, imaging views and clinical utility, 1077

regurgitant orifice
color Doppler velocity accuracy proximal to regurgitant orifices: influence of orifice aspect ratio (Myers), 771
morphological evaluation of a regurgitant orifice by 3-D echocardiography: applications in the quantification of valvular regurgitation (Anayiotos), 209

Reid, G., see Markus, H. S.
Reilly, C. F., see Allott, C. P.
Reimers, C. D., see Heinemeyer, O.
Remenieras, J.-P., see Guittet, C.

renal artery
a validation study on the intraobserver and interobserver reproducibility of renal artery duplex ultrasound (Baumgartner), 225

renal cell carcinoma
early detection of renal cell carcinoma by ultrasonographic screening - based on the results of 13 years screening in Japan (Mihara), 1033

Reneman R. S., see Willekes, C.
Reneman, R. S., see Willekes, C.

reproducibility
a validation study on the intraobserver and interobserver reproducibility of renal artery duplex ultrasound (Baumgartner), 225
an *in vivo* evaluation of the reproducibility of intima-media thickness measurements of the carotid artery segments using B-mode ultrasound (Montauban van Swijndregt), 323
artificial neural network analysis of common femoral artery Doppler shift signals: classification of proximal disease (Wright), 735
clinical implications of online and off-line interobserver variability in intracoronary ultrasound-guided interventions (Smits), 509
variability in ultrasonic measurements of arterial stiffness in the atherosclerosis risk in communities study (Arnett), 175

reproductive events
relationship of thyroid blood flow to reproductive events in normal Chinese females (Chan), 233

Resnick, M. B., see Shupak, A.

response
transvaginal color Doppler for predicting pathological response to preoperative chemoradiation in locally advanced cervical carcinoma: a preliminary study (Alcázar), 1041

reviews, book
abdominal ultrasound principles and techniques (Freeman), 315
an atlas of neonatal brain sonography (Stringfellow), 319
cardiac ultrasound (Wilde), 317
contrast ultrasound for the radiologist (Dawson), 316
diagnostic ultrasound (Dewbury), 863
diagnostic ultrasound of fetal anomalies (in compact disk) (Smith), 1475
guidelines and gamuts in musculoskeletal ultrasound (King), 1019
obstetric ultrasound: principles and techniques (Dubbins), 316
ophthalmic ultrasound: a diagnostic atlas (Trier), 1159
ultrasonic instruments and devices – I (Preston), 491
ultrasound teaching manual: the basics of performing and interpreting ultrasound scans (Edie), 863
vascular diagnosis with ultrasound (Oates), 487

Resnick, M. B., see Shupak, A.
Rickey, D. W., see Kulbisky, G. P.
Riederer, P., see Berg, D.
Righetti, R., Kallel, F., Stafford, R. J., Price, R. E., Krouskop, T. A., Hazle, J. D. and Ophir, J.: elastographic characterization of HIFU-induced lesions in canine livers, 1099
Righetti, R., see Kallel, F.
Riley, W., see Arnett, D. K.
Roatta, S., see Guiot, C.
Robertson, D., see Chen, L.
Rohner, P., see Baumgartner, I.
Ronco, A. L. and Fernandez, R.: improving ultrasonographic diagnosis of prostate cancer with neural networks, 729
Rosenhause, G., see Shupak, A.
Rotteveel, J. J., see Mullaart, R. A.,
Roubidoux, M. A., see Meyer, C. R.
Routh, H. F., see Ramnarine, K. V.
Roy, E., Montrésor, S., Abraham, P. and Saumet, J.-L.: spectrogram analysis of arterial Doppler signals for off-line automated hits detection, 349
Rubin, J. M., see Tuthill, T. A.
Ryaby, J. T., see Luo, G.
Rywik, T. M., see Nagai, Y.
Rywik, T. M., see Nagai, Y.

S

Saccomandi, F., see Guiot, C.

safety
a comparison of AIUM/NEMA thermal indices with calculated temperature rises for a simple third-trimester pregnancy tissue model (Jago), 623
acoustic saturation and output regulation (Duck), 1009
angular directivity of thermal coagulation using air-cooled direct-coupled interstitial ultrasound applicators (Deardorff), 609
hemorrhage in murine fetuses exposed to pulsed ultrasound (Dalecki), 1139
in vitro heating of human fetal vertebra by pulsed diagnostic ultrasound (Doody), 1289
in vivo demonstration of noninvasive thermal surgery of the liver and kidney using an ultrasonic phased array (Daum), 1087

intercomparison of acoustic output measurements of a diagnostic ultrasound device (Beissner), 529
low-frequency, low-intensity ultrasound accelerates thrombolysis through the skull (Behrens), 269
production of harmonics *in vitro* by high-intensity focused ultrasound (Clarke), 1417
rationale and derivation of MI and TI – a review (Abbott), 431
sonochemically induced radicals generated by pulsed high-energy ultrasound *in vitro* and *in vivo* (Debus), 301
temperature elevation computed for three-layer and four-layer obstetrical tissue models in nonlinear and linear propagation cases (Filipczynski), 865 (Erratum)
temperature elevations computed for three-layer and four-layer obstetrical tissue models in nonlinear and linear ultrasonic propagation cases (Wójcik), 259
transient poration and cell surface receptor removal from human lymphocytes *in vitro* by 1 MHz ultrasound (Brayman), 999
ultrasound power deposition model for the chest wall (Moros), 1275
ultrasound technology for hyperthermia (Diederich), 871 (Review Article)
ultrasound-induced cavitation damage to external epithelia of fish skin (Frenkel), 1295

Sagiv, C., Akselrod, S. and Tepper, R.: application of a semiautomatic boundary detection algorithm for the assessment of amniotic fluid quantity from ultrasound images, 515
Sakamoto, H., see Masugata, H.
Sakamoto, S., see Masugata, H.
Salvesen, K. Å. and Eik-Nes, S. H.: ultrasound during pregnancy and birthweight, childhood malignancies and neurological development, 1025 (Review Article)
Samstad, S., see Berg, S.
Saumet, J.-L., see Abraham, P.
Saumet, J.-L., see Roy, E.
Scheld, H. H., see Kohl, T.
Schild, R. L., see Wallny, T. A.
Schima, H., see Porenta, G.
Schlief, R., see Blomley, M. J. K.
Schmitt, O., see Wallny, T. A.
Schroeck, H., see Els, T.
Schuurman, P. R. and Albrecht, K. W.: intraoperative changes of transcranial Doppler velocity: relation to arterial oxygen content and whole-blood viscosity, 151
Schwartzman, D., see Ren, J.-F.

screening
early detection of renal cell carcinoma by ultrasonographic screening - based on the results of 13 years screening in Japan (Mihara), 1033

Seki, M., see Mizushige, K.
Senda, S., see Masugata, H.
Serizawa, M., see Maeda, K.
Shau, Y.-W., Wang, C.-L., Shieh, J.-Y. and Hsu, T.-C.: noninvasive assessment of the viscoelasticity of peripheral arteries, 1377
Shaw, A., Pay, N. M., Preston, R. C. and Bond, A. D.: proposed standard thermal test object for medical ultrasound, 121

Sherriff, S. B., see Walker, R. D.
Shi, W. T., Forsberg, F., Raichlen, J. S., Needleman, L. and Goldberg, B. B.: pressure dependence of subharmonic signals from contrast microbubbles, 275
Shi, W. T., see Forsberg, F.
Shieh, J.-Y., see Shau, Y.-W.
Shih, J. C., see Peng, S. S.-F.

shock waves
a comparison of shock wave and sinusoidal-focused ultrasound-induced localized transfection of HeLa cells (Huber), 1451
acoustic saturation and output regulation (Duck), 1009
effect of high-intensity focused ultrasound on whole blood with and without microbubble contrast agent (Poliachik), 991
effect of macroscopic air bubbles on cell lysis by shock wave lithotripsy *in vitro* (Williams), 473

Shun, C.-T., see Kuo, P.-L.
Shung, K. K., see Lin, Y.-H.
Shung, K. K., see Missaridis, T. X.
Shupak, A., Arieli, R., Rosenhause, G., Resnick, M. B., Arieli, Y. and Adir, Y.: the effect of low-frequency ultrasound on immersed pig lungs, 1439
Siffert, R. S., see Luo, G.
Silverman, N. H., see Kohl, T.
Simon, A., see Graf, S.
Sirlin, C. B., Girard, M. S., Baker, K. G., Steinbach, G. C., Deiranieh, L. H. and Mattrey, R. F.: effect of acquisition rate on liver and portal vein enhancement with microbubble contrast, 331

skin
high-frequency estimation of the ultrasonic attenuation coefficient slope obtained in human skin: simulation and *in vivo* results (Guittet), 421
ultrasound-induced cavitation damage to external epithelia of fish skin (Frenkel), 1295

Slager, C. J., see Krams, R.

small bowel
contrast ultrasonography of the normal small bowel (Pallotta), 1335

Smith, A. P. M.: diagnostic ultrasound of fetal anomalies (in compact disk), 1475
Smith, B. K., see Anayiotos, A. S.,
Smith, N. B., see Daum, D. R.
Smith, R. E., see Walker, R. D.
Smits, P. C., Pasterkamp, G., Eefting, F. D., Stella, P. R., de Jaegere, P. P. T. and Borst, C.: clinical implications of online and off-line interobserver variability in intracoronary ultrasound-guided interventions, 509
Sobanski, M. A., see Thomas, N. E.

sound speed
relationship between myocardial tissue density measured by microgravimetry and sound speed measured by acoustic microscopy (Masugata), 1459 (Clinical Note)

Spaan, J. A. E., see Bos, L. J.

spectral broadening
finite beam-width ray model for geometric spectral broadening (Hoskins), 391

spectral width Doppler
implementation of spectral width Doppler in pulsatile flow measurements (Lee), 1221

Spiegel, D., see Behrens, S.

spinal canal
the fetal spinal canal - a three-dimensional study (Wallny), 1329

Spoo, J., see Debus, J.
Stafford, R. J., see Kallel, F.
Stafford, R. J., see Righetti, R.
Stam, H. J., see Holland, W. P. J.

standards
a comparison of AIUM/NEMA thermal indices with calculated temperature rises for a simple third-trimester pregnancy tissue model (Jago), 623
acoustic saturation and output regulation (Duck), 1009
intercomparison of acoustic output measurements of a diagnostic ultrasound device (Beissner), 529
proposed standard thermal test object for medical ultrasound (Shaw), 121
rationale and derivation of MI and TI – a review (Abbott), 431

standing wavea
ultrasonic enhancement of coated particle agglutination immunoassays: influence of particle density (Thomas), 443

Steen, E., see Berg, S.
Steinbach, G. C., see Sirlin, C. B.
Stella, P. R., see Smits, P. C.

stenoses
accuracy of the main Doppler methods for evaluating the degree of carotid stenoses (continuous wave, pulsed wave, and color Doppler), (Arbeille), 65
noninvasive 3-D ultrasound of atherosclerotic plaques in the Watanabe rabbit (Allott), 905
review of the assessment of single level and multilevel arterial occlusive disease in lower limbs by duplex ultrasound (Allard), 495

stereotactic positioning
design considerations for a transcranial Doppler coupled to a stereotactic position arm (Mignault), 111

Stewart, S. F. C.: a rotating torus phantom for assessing color Doppler accuracy, 1251
Stonehill, M. A., see Williams, J. C. Jr.
Stonehill, M. A., see Williams, J. C. Jr. Stöver, B., see Nagdyman, N.

strain
strain measurements of rabbit Achilles tendons by ultrasound (Kuo), 1241
tendon displacement assessment by pulsed Doppler tissue imaging: validation with a reciprocating string test target (Holland), 1229

Straube, W. L., see Moros, E. G.
Strauss, A. L. and Beller, K.-D.: persistent opacification of the left ventricle and myocardium with a new echo contrast agent, 763
Strelitzki, R., Metcalfe, S. C., Nicholson, P. H. F., Evans, J. A. and Paech, V.: on the ultrasonic attenuation and its frequency dependence in the Os Calcis assessed with a multielement receiver, 133
Stringfellow, J. M.: an atlas of neonatal brain sonography, 319
Strohmer, T., see Binder, T.

substantia nigra
iron accumulation in the substantia nigra in rats visualized by ultrasound (Berg), 901

Suda, K., see Kohl, T.
Suetens, P., see Bijnens, B.
Sugimoto, S., see Kodama, T.

surgery
does venous microemboli detection add to the interpretation of D-dimer values following orthopedic surgery?, (Abraham) 637 (Clinical Note)
low-frequency, low-intensity ultrasound accelerates thrombolysis through the skull (Behrens), 269

Süssner, M., see Binder, T.
Sutherland, G., see Bijnens, B.

T

Tadaoka, S., see Kagiyama, M.
Takayama, K., see Kodama, T.
Tatsuno, M., see Kodama, T.
Taylor, K. J. W., see Brown, J. M.

tendon
frequency analysis of echo texture in tendon (Tuthill), 959
strain measurements of rabbit Achilles tendons by ultrasound (Kuo), 1241
tendon displacement assessment by pulsed Doppler tissue imaging: validation with a reciprocating string test target (Holland), 1229

Tepper, R., see Sagiv, C.
Tepper, R., see Zimmer, Y.
Ternisien, C., see Abraham, P.

texture
frequency analysis of echo texture in tendon (Tuthill), 959

thermal effects
angular directivity of thermal coagulation using air-cooled direct-coupled interstitial ultrasound applicators (Deardorff), 609

heating vs. cavitation in the induction of mouse hindlimb paralysis by ultrasound (Miller), 1145
in vitro heating of human fetal vertebra by pulsed diagnostic ultrasound (Doody), 1289
in vivo demonstration of noninvasive thermal surgery of the liver and kidney using an ultrasonic phased array (Daum), 1087
proposed standard thermal test object for medical ultrasound (Shaw), 121
temperature elevation computed for three-layer and four-layer obstetrical tissue models in nonlinear and linear propagation cases (Filipczynski), 865 (Erratum)
temperature elevations computed for three-layer and four-layer obstetrical tissue models in nonlinear and linear ultrasonic propagation cases (Wójcik), 259
the feasibility of elastographic visualization of HIFU-induced thermal lesions in soft tissues (Kallel), 641 (Technical Note)
ultrasound power deposition model for the chest wall (Moros), 1275
ultrasound technology for hyperthermia (Diederich), 871 (Review Article)

thermal indices
a comparison of AIUM/NEMA thermal indices with calculated temperature rises for a simple third-trimester pregnancy tissue model (Jago), 623
proposed standard thermal test object for medical ultrasound (Shaw), 121
rationale and derivation of MI and TI – a review (Abbott), 431
temperature elevation computed for three-layer and four-layer obstetrical tissue models in nonlinear and linear propagation cases (Filipczynski), 865 (Erratum)
temperature elevations computed for three-layer and four-layer obstetrical tissue models in nonlinear and linear ultrasonic propagation cases (Wójcik), 259
ultrasound power deposition model for the chest wall (Moros), 1275
ultrasound technology for hyperthermia (Diederich), 871 (Review Article)

Thijssen, J. M., see Mullaart, R. A.,
Thomas, N. E., Sobanski, M. A. and Coakley, W. T.: ultrasonic enhancement of coated particle agglutination immunoassays: influence of particle density, 443
Thomson, D. S., see Allott, C. P.
Thrall, B. D., see Miller, D. L.

thyroid
relationship of thyroid blood flow to reproductive events in normal Chinese females (Chan), 233

tissue characterisation
computational methods for ultrasonic bone assessment ((Luo), 823
computerized quantification of structures within ovarian cysts using ultrasound images (Zimmer), 189
echogenicity of fetal lung and liver quantified by the grey-level histogram width (Maeda), 201
experimental investigation of the acoustic nonlinearity parameter tomography for excised pathological biological tissues (Zhang), 593
frequency analysis of echo texture in tendon (Tuthill), 959
high-frequency estimation of the ultrasonic attenuation coefficient slope obtained in human skin: simulation and *in vivo* results (Guittet), 421

nonlinear and linear propagation of diagnostic ultrasound pulses (Filipczynski), 285
nonlinearity parameter for tissue-mimicking materials (Dong), 831
on the relation between aggregation, packing and the backscattered ultrasound signal for whole blood (Lim), 1395
on the ultrasonic attenuation and its frequency dependence in the Os Calcis assessed with a multielement receiver (Strelitzki), 133
quantitative ultrasonography of the perventricular white and grey matter of the developing brain (Mullaart), 527
robustness of integrated backscatter for myocardial tissue characterization (Bijnens), 95
ultrasonic propagation in cancellous bone: a new stratified model (Hughes), 811
ultrasound backscatter and attenuation in human liver with diffuse disease (Lu), 1047
wide-band spectroscopy of biological material based on a laser-induced grating technique (Maznev), 601

tissue harmonic imaging
clinical use of ultrasound tissue harmonic imaging (Tranquart), 889
nonlinear and linear propagation of diagnostic ultrasound pulses (Filipczynski), 285
nonlinearity parameter for tissue-mimicking materials (Dong), 831

Titulaer, B. M., see Mess, W. H.
Todros, T., see Guiot, C.

tomography
experimental investigation of the acoustic nonlinearity parameter tomography for excised pathological biological tissues (Zhang), 593

Torp, H., see Berg, S.
Toyka, K. V., see Müllges, W.

trabecular bone
computational methods for ultrasonic bone assessment ((Luo), 823

Tranquart, F., Grenier, N., Eder, V. and Pourcelot, L.: clinical use of ultrasound tissue harmonic imaging, 889

transcranial Doppler
design considerations for a transcranial Doppler coupled to a stereotactic position arm (Mignault), 111
effect of ECHO contrast media on the visualization of transverse sinus thrombosis with transcranial 3-D duplex sonography (Delcker), 1063
intraoperative changes of transcranial Doppler velocity: relation to arterial oxygen content and whole-blood viscosity (Schuurman), 151

transfection
a comparison of shock wave and sinusoidal-focused ultrasound-induced localized transfection of HeLa cells (Huber), 1451
ultrasonic enhancement of gene transfection in murine melanoma tumors (Miller), 1425

transesophageal echocardiography
fetal transesophageal echocardiography utilizing a 10-F, 10-MHz intravascular ultrasound catheter – comparison with conventional maternal transabdominal fetal echocardiography in sheep (Kohl), 939

transverse sinus thrombosis
effect of ECHO contrast media on the visualization of transverse sinus thrombosis with transcranial 3D duplex sonography (Delcker), 1063

Trier, H. G.: ophthalmic ultrasound: a diagnostic atlas, 1159
Tsangaris, S., see Porenta, G.
Tsao, P.-N., see Peng, S. S.-F.
Tsou, K.-I. Y., see Peng, S. S.-F.

tumour blood flow
kinetic study of tumor blood flow in prostatic cancer using power Doppler imaging (Okihara), 89
transvaginal color Doppler for predicting pathological response to preoperative chemoradiation in locally advanced cervical carcinoma: a preliminary study (Alcázar), 1041

Tuthill, T. A., Rubin, J. M., Fowlkes, J. B., Jamadar, D. A. and Bude, R. O.: frequency analysis of echo texture in tendon, 959
Tymkiewicz, R., see Filipczynski, L.
Tymkiewicz, R., see Filipczynski, L.

U

Uchimoto, R., Niwa, K., Eguchi, H., Kamiyama, N., Mine, Y., Miyazawa, T. and Brautigam, M.: *in vivo* kinetics of microbubbles of SH U 508 A (Levovist®): comparison with Indocyanine Green in rabbits, 1365
Ueda, T., see Mizushige, K.
Uenohara, H., see Kodama, T.

ultrasound guidance
clinical implications of online and off-line interobserver variability in intracoronary ultrasound-guided interventions (Smits), 509
contrast-enhanced ultrasound for guidance of local tumor ablation (Brown), 1213
hemostasis of punctured vessels using Doppler-guided high-intensity ultrasound (Martin), 985

ultrasound velocity
computational methods for ultrasonic bone assessment ((Luo), 823
ultrasonic propagation in cancellous bone: a new stratified model (Hughes), 811
ultrasound backscatter and attenuation in human liver with diffuse disease (Lu), 1047
wide-band spectroscopy of biological material based on a laser-induced grating technique (Maznev), 601

umbilical flow
umbilical arterial blood flow in the mouse embryo during development and following acutely increased heart rate (MacLennan), 361

Uren, N. G., see Komiyama, N.
Utsu, M., see Maeda, K.,

V

Vaezy, S., see Takayama, K.
Vaidya, S., see Brayman, A. A.
Valckx, F. M., see Mullaart, R. A.,

valvular regurgitation
morphological evaluation of a regurgitant orifice by 3-D echocardiography: applications in the quantification of valvular regurgitation (Anayiotos), 209

Van de Werf, F., see Bijnens, B.
van der Steen, A. F. W., see Krams, R.
van der Steen, A. F. W., see Li, W.
van Geemen, A. J., see Mullaart, R. A.,
Van Kaick, G., see Delorme, S.
Varghese, T., see Konofagou, E. E.

velocity
a comparison of single- and dual-beam methods for maximum velocity estimation (Hoskins), 583
a rotating torus phantom for assessing color Doppler accuracy (Stewart), 1251
artificial neural network analysis of common femoral artery Doppler shift signals: classification of proximal disease (Wright), 735
increased accuracy of echocardiographic measurement of flow using automated spherical integration of multiple plane velocity vectors (Brandberg), 249
measurement accuracy of the flow velocity in pulsed ultrasound Doppler velocimeter (Kagiyama), 1265
portal venous volume flow: *in vivo* measurement by time-domain color-velocity imaging (Kawasaki), 915
sensitivity of color Doppler sonography: an experimental approach (Delorme), 541
time-averaged mean velocity for volumetric blood flow measurements: an *in vitro* model validation study using physiological femoral artery flow waveforms (Walker), 577

ventricular function
artificial neural networks and spatial temporal contour linking for automated endocardial contour detection on echocardiograms: a novel approach to determine left ventricular contractile function (Binder), 1069

Vergroesen, I., see Bos, L. J.
Vinke, R., see Krams, R.
Vogt, J., see Kohl, T.
Vray, D., see Delachartre, P.

W

Wagner, U. A., see Wallny, T. A.
Walka, M. M., see Nagdyman, N.
Walker, R. D., Smith, R. E., Sherriff, S. B. and Wood, R. F. M.: time-averaged

mean velocity for volumetric blood flow measurements: an *in vitro* model validation study using physiological femoral artery flow waveforms, 577
Wallny, T. A., Schild, R. L., Fimmers, R., Wagner, U. A., Hansmann, M. E. and Schmitt, O.: the fetal spinal canal - a three-dimensional study, 1329
Wang, C.-L., see Shau, Y.-W.
Wang, J.-H., see Lee, B.-R.
Wang, W., see Liu, B.
Wang, Y., see Liu, B.
Wannenmacher, M. F., see Huber, P. E.
Watanabe, H., see Okihara, K.

wavelet
spectrogram enhancement algorithm: a soft thresholding-based approach (Liu), 839
the use of the wavelet transform to describe embolic signals (Aydin), 953

Weimar, C., see Delcker, A.
Wentzel, J. J., see Krams, R.
Wesemann, W., see Berg, D.
Wheatley, M. A., see Forsberg, F.
White, P. R., see Hughes, E. R.
Whittingham, T. A., see Jago, J. R.
Wijn, P., see Nagai, Y.
Wilde, P.: cardiac ultrasound, 317
Willekes, C., Hoeks, A. P. G., Bots, M. L., Brands, P. J., Willigers, J. M. and Reneman R. S.: evaluation of off-line automated intima-media thickness detection of the common carotid artery - based on M-line signal processing, 57
Willekes, C., Hoogland, H. J., Keizer, H. A., Hoeks, A. P. G. and Reneman, R. S.: three months use of third-generation oral contraceptives does not affect artery wall properties, 723
Williams, J. C. Jr., Stonehill, M. A., Colmenares, K., Evan, A. P., Andreoli, S. P., Cleveland, R. O., Bailey, M. R., Crum, L. A. and McAteer, J. A.: effect of macroscopic air bubbles on cell lysis by shock wave lithotripsy *in vitro*, 473
Williams, J. C. Jr., Woodward, J. F., Stonehill, M. A., Evan, A. P. and McAteer, J. A.: cell damage by lithotripter shock waves at high pressure to preclude cavitation, 1445
Willigers, J. M., see Willekes, C.

Windkessel
decay index: a new carotid Doppler waveform measure associated with the Windkessel function of elastic arteries (Nagai), 1371

Wójcik, J., Filipczynski, L. and Kujawska, T.: temperature elevations computed for three-layer and four-layer obstetrical tissue models in nonlinear and linear ultrasonic propagation cases, 259
Wójcik, J., see Filipczynski, L.
Wójcik, J., see Filipczynski, L.
Wood, A. K. W., see Wright, A. B.
Wood, R. F. M., see Walker, R. D.
Woodward, J. F., see Williams, J. C. Jr.
Wright, A. B., McKelvey, G. M., Wood, A. K. W. and Post, E. J.: effects of

promethazine on porcine gastroduodenal function: a sonographic study, 241
Wright, I. A. and Gough, N. A. J.: artificial neural network analysis of common femoral artery Doppler shift signals: classification of proximal disease, 735
Wu, C.-C., see Liu, Y.-B.

Y

Yamamoto, N., see Maeda, K.
Ying, M., Ahuja, A., Brook, F., Brown, B. and Metreweli, C.: nodal shape (S/L) and its combination with size for assessment of cervical lymphadenopathy: which cut-off should be used?, 1169
Yock, P. G., see Komiyama, N.
Yoshimoto, T., see Kodama, T.
Yoshioka, R., see Mihara, S.
Yuba, M., see Mizushige, K.

Z

Zagzebski, J. A., see Dong, F.
Zagzebski, J. A., see Lu, Z. F.
Zhang, D. and Gong, X.-F.: experimental investigation of the acoustic nonlinearity parameter tomography for excised pathological biological tissues, 593
Zimmer, Y., Tepper, R. and Akselrod, S.: computerized quantification of structures within ovarian cysts using ultrasound images, 189
Zuna, I., see Delorme, S.